NASA/TM–2025–104606/Vol. 66

Technical Report Series on Global Modeling and Data Assimilation, Volume 66

TBD, Editor

Validation Assessment for the Soil Moisture Active Passive (SMAP) Level 4 Carbon (L4_C) Data Product Version 8

K. Arthur Endsley, John S. Kimball, Tobias Kundig, Rolf H. Reichle, Joseph V. Ardizzone

October 2025

NASA STI Program ... in Profile

Since its founding, NASA has been dedicated to the advancement of aeronautics and space science. The NASA scientific and technical information (STI) program plays a key part in helping NASA maintain this important role.

The NASA STI program operates under the auspices of the Agency Chief Information Officer. It collects, organizes, provides for archiving, and disseminates NASA's STI. The NASA STI program provides access to the NTRS Registered and its public interface, the NASA Technical Reports Server, thus providing one of the largest collections of aeronautical and space science STI in the world. Results are published in both non-NASA channels and by NASA in the NASA STI Report Series, which includes the following report types:

- TECHNICAL PUBLICATION. Reports of completed research or a major significant phase of research that present the results of NASA Programs and include extensive data or theoretical analysis. Includes compilations of significant scientific and technical data and information deemed to be of continuing reference value. NASA counterpart of peer-reviewed formal professional papers but has less stringent limitations on manuscript length and extent of graphic presentations.

- TECHNICAL MEMORANDUM. Scientific and technical findings that are preliminary or of specialized interest, e.g., quick release reports, working papers, and bibliographies that contain minimal annotation. Does not contain extensive analysis.

- CONTRACTOR REPORT. Scientific and technical findings by NASA-sponsored contractors and grantees.

- CONFERENCE PUBLICATION. Collected papers from scientific and technical conferences, symposia, seminars, or other meetings sponsored or co-sponsored by NASA.

- SPECIAL PUBLICATION. Scientific, technical, or historical information from NASA programs, projects, and missions, often concerned with subjects having substantial public interest.

- TECHNICAL TRANSLATION. English-language translations of foreign scientific and technical material pertinent to NASA's mission.

Specialized services also include organizing and publishing research results, distributing specialized research announcements and feeds, providing information desk and personal search support, and enabling data exchange services.

For more information about the NASA STI program, see the following:

- Access the NASA STI program home page at http://www.sti.nasa.gov

- E-mail your question to help@sti.nasa.gov

- Phone the NASA STI Information Desk at 757-864-9658

- Write to:
  NASA STI Information Desk
  Mail Stop 148
  NASA Langley Research Center
  Hampton, VA 23681-2199

NASA/TM–2023–104606/Vol. 66

Technical Report Series on Global Modeling and Data Assimilation, Volume 66

TBD, Editor

Validation Assessment for the Soil Moisture Active Passive (SMAP) Level 4 Carbon (L4_C) Data Product Version 8

K. Arthur Endsley
University of Montana, Missoula, MT, USA.

John S. Kimball
University of Montana, Missoula, MT, USA.

Tobias Kundig
University of Montana, Missoula, MT, USA.

Rolf H. Reichle
Global Modeling and Assimilation Office, NASA Goddard Space Flight Center, Greenbelt, MD, USA.

Joseph V. Ardizzone
Science Systems and Applications Inc., Lanham, MD, USA.

National Aeronautics and
Space Administration

Goddard Space Flight Center
Greenbelt, Maryland 20771

October 2025

Level of Review: This material has been technically reviewed by technical management.

Available from

NASA STI Program
Mail Stop 148
NASA's Langley Research Center Hampton, VA 23681-2199

National Technical Information Service
5285 Port Royal Road
Springfield, VA 22161
703-605-6000

Table of Contents

1 Executive Summary

The NASA Soil Moisture Active Passive (SMAP) mission has recently completed its first decade of continuous, global measurements of Earth's L-band (1.4 GHz) microwave emission (or brightness temperature), which began on 31 March 2015. Starting even before launch, periodic calibration and validation activities have been performed with the objectives: 1) To calibrate, verify, and improve the performance of the science algorithms; and 2) To validate the accuracy of the science data products as specified in the SMAP Level 1 mission science requirements.

This report provides an assessment of Version 8 (V8) of the SMAP Level 4 Carbon (L4_C) product, which was released in 2025. Since the initial L4_C release in 2015, the L4_C operational algorithm underwent eight major updates, with each update including a full reprocessing of the entire SMAP mission record. These updates include various algorithm refinements and calibration adjustments to account for similar refinements to upstream SMAP brightness temperature observations, the GEOS land model assimilation system, and the SMAP Level 4 Soil Moisture (L4_SM) inputs used for L4_C processing. In addition, the L4_C V8 update includes major changes to the L4_C calibration process, the soil organic carbon (SOC) model logic, and the soil heterotrophic respiration (R_H) sub-model.

The L4_C algorithm estimates a global, daily terrestrial carbon budget, informed by daily surface and root-zone soil moisture information from the L4_SM product, along with optical remote sensing-based land cover from the Moderate Resolution Imaging Spectroradiometer (MODIS) and canopy fraction of absorbed photosynthetically active radiation (fPAR) from the Visible Infrared Imaging Radiometer Suite (VIIRS), along with other ancillary biophysical data. The L4_C product provides estimates of global, daily net ecosystem CO_2 exchange (NEE) and component carbon fluxes, including vegetation gross primary production (GPP) and soil R_H. Other L4_C product elements include surface (ca. 0-5 cm depth) SOC stocks and associated environmental constraints to the carbon fluxes, including soil moisture-related controls on GPP and ecosystem respiration (RECO) (Kimball et al. 2014; Jones et al. 2017).

The L4_C product addresses SMAP carbon cycle science objectives by: 1) Providing a direct link between terrestrial carbon fluxes and underlying freeze/thaw and soil moisture-related constraints to these processes; 2) Documenting primary connections between terrestrial water, energy and carbon cycles; and 3) Improving understanding of terrestrial carbon sink activity.

L4_C is calibrated against eddy covariance (EC) tower CO_2 flux measurements, which are a proxy for terrestrial ecosystem NEE. The L4_C product has self-imposed performance requirements related to NEE, the primary product element for validation, although the other L4_C product elements (namely GPP, R_H, and SOC) have demonstrated utility for carbon science applications (Liu et al. 2019; Endsley et al. 2020; Wurster et al. 2021; Xia et al. 2025). The L4_C targeted accuracy requirement is a mean unbiased root-mean-square error (ubRMSE, or standard deviation of the error) for NEE

of no more than 1.6 g C $m^{-2}d^{-1}$ or 30 g C m^{-2} yr^{-1}, emphasizing northern ($\geq 45°N$) boreal and arctic ecosystems; this accuracy is similar to that of EC tower flux measurements (Baldocchi 2008). The methods used for L4_C performance and validation assessment have been established in the SMAP Calibration and Validation Plan (Colliander et al. 2014) and previous studies (Jones et al. 2017; Endsley et al. 2020), and are applied here for L4_C V8.

Our primary validation of L4_C V8 compares L4_C estimates of NEE, GPP, and RECO to tower flux measurements at 26, globally distributed Core Validation Sites. We also compared the L4_C V8 mean annual fluxes, interannual variability, and short-term trends to the recent literature and to independent reference datasets, including: solar-induced fluorescence (SIF) data from the Orbiting Carbon Observatory-2 (OCO-2) mission; global, up-scaled EC tower fluxes from an ensemble of machine-learning models; global soil carbon inventory records; and an ensemble of dynamic global vegetation models.

2 L4_C Algorithm Updates in Version 8

As with previous reprocessing of upstream SMAP products, Version 8 (V8) of the SMAP Level 4 Carbon (L4_C) product incorporates changes made to its inputs, especially data from the SMAP Level 4 Soil Moisture (L4_SM) product. The L4_SM V8 upgrade improved the L4_SM precipitation inputs, land surface model, and L-band microwave radiative transfer model which, in turn, impact the L4_SM estimates of root-zone soil moisture, surface soil moisture, and surface soil temperature that are used to generate the L4_C V8 product. To accommodate these changes, L4_C V8 was recalibrated using L4_SM Nature Run version 11.4 (NRv11.4), a multi-decadal, model-only representation of L4_SM V8 that is not informed by SMAP brightness temperature retrievals but is climatologically consistent with the L4_SM V8 product.

In addition to the aforementioned updates of the L4_C algorithm inputs, major changes were made to the L4_C calibration process, SOC model logic, and the R_H sub-model. L4_C calibration now utilizes both constrained non-linear optimization and Markov Chain Monte Carlo (MCMC) methods, where the latter is used to incorporate prior data on model parameters into the calibration process (Endsley et al. 2023b). The motivation for this change was specifically to improve the plant carbon use efficiency (CUE) parameter in L4_C, which determines the (fixed) fraction of autotrophic respiration (R_A) which, added to R_H, makes up RECO and can be calibrated against tower observations. In previous versions of L4_C, plant CUE was fairly high (between 0.65 and 0.80 for most PFTs in V7), leading to a compensatory over-estimation of R_H and net primary productivity (NPP). A comprehensive meta-analysis by Collalti and Prentice (2019) suggests that the valid range for CUE spans 0.22-0.79, with a cross-biome average of 0.46±0.12 (standard deviation). Hence, we used their data as a prior for CUE during calibration, and the V8 CUE values are now lower (between 0.50 and 0.58).

In the SOC model, we substantially changed the allocation of litterfall to the soil in order to address an outstanding model bias. It has been shown that in earlier versions of L4_C, as in similar global ecosystem models, the seasonal cycles of RECO and NEE exhibit a bias towards earlier peak (maximum) RECO and delayed peak (minimum) NEE, when compared to EC tower data (Byrne et al. 2018; Endsley et al. 2022). This phase shift in the modeled seasonal cycles of RECO and NEE can be corrected by suppressing early season respiration or by prolonging respiration throughout the growing season. There are a few mechanisms that can effect these changes in terrestrial ecosystems, e.g., the suppression of R_A in the light and the slow diffusion of heat and moisture in soils. In Endsley et al. (2022), it was demonstrated that a more realistic litterfall phenology could also correct this seasonal bias. In previous versions of L4_C, litterfall was prescribed as a constant, daily fraction of annual NPP, allocated equally throughout the year. This may have been the primary cause of the observed seasonal bias in respiratory carbon fluxes. In L4_C V8, we have adopted the leaf-loss function of the Carnegie-Ames-Stanford Approach (CASA) model, using a climatology of VIIRS

VNP15 leaf-area index (LAI), which determines how much litterfall to allocate for each 8-day period in the calendar year.

In addition to the change in litterfall, new ground data on SOC content from the International Soil Carbon Network (ISCN) were used to calibrate the SOC decay coefficients. Calibration of these coefficients remains subjective, as we would not expect a good fit between L4_C predictions and the full domain of field-measured SOC. There are two main reasons why we, instead, fit a line through the lower-magnitude field samples: 1) L4_C does not represent important SOC protection mechanisms that help to prevent SOC decomposition; 2) The SOC decomposition and R_H sub-model is driven by near-surface temperature and moisture conditions, which are highly dynamic and, consequently, lead to rapid SOC decay. The new ISCN data, nonetheless, represent a much larger spatial domain and are expected to be of higher quality than the previous SOC calibration data.

As with previous re-processing events, we also recalibrated the L4_C model Biome Properties Look-up Table (BPLUT) by optimizing L4_C predicted GPP and RECO fluxes against observed GPP and RECO fluxes from a global network of eddy covariance flux towers (Pastorello et al. 2020; Ukkola et al. 2021). For L4_C V8, we have developed a new calibration dataset consisting of 410 globally distributed EC towers (compared to 356 in V7), because the previously used FLUXNET2015 dataset has become outdated (Pastorello et al. 2020). We also had our own concerns about excessive smoothing in FLUXNET2015. The new calibration data were obtained individually, for each tower, and span multiple tower networks including: FLUXNET and AmeriFlux (Pastorello et al. 2020), the Arctic Data Center (Euskirchen et al. 2016a, 2016b, 2016c), the Global Environmental Database from Japan's National Institute for Environmental Studies (NIES-GED) (Takagi 2014; Takahashi 2021; Hirata 2021), OzFlux (Leuning et al. 2005; Woodgate 2013; Beringer et al. 2016; Wardlaw and Phillips 2021), the European Fluxes Database Cluster (Papale et al. 2006), and select towers in Brazil from the Large Scale Biosphere-Atmosphere Experiment (LBA-ECO) (Restrepo-Coupe et al. 2021).

In all cases, we prioritized the use of half-hourly flux data partitioned by the tower's principal investigator (PI) and avoided gap-filled data. Most FLUXNET and AmeriFlux towers provided NEE data that was quality-controlled using the Variable Ustar Threshold (VUT) for each year. If replicates were provided, we averaged among sensors at the same height above the canopy. Tower fluxes were then converted from CO_2 to carbon mass flux and aggregated to daily time steps in one of two ways: if there are no missing (hourly or half-hourly) measurements in a day, the daily sum is obtained; otherwise, a daily mean is taken and then scaled to a daily total. The updated fluxes were used in the calibration protocol established in the previous re-processing (Endsley et al. 2023b), to obtain the updated BPLUT. Following recalibration of the BPLUT, the L4_C initial SOC pool sizes were initialized as described by Jones et al. (2017), based on updated L4_SM soil moisture and temperature climatologies.

Unless noted otherwise, the L4_C V8 product examined in the present report is from Science Version ID Vv8040 (31 March 2015 – 30 September 2024) and Vv8041 (1

October 2024 – present), which were released in July 2025 as part of a minor version upgrade to address a transient bias discovered in the original L4_C V8 release of April 2025 (Science Version IDs Vv8020 and Vv8021; see section 3.4).

3 L4_C Product Performance at SMAP Core Validation Sites

The primary validation of the L4_C product consists of its assessment against carbon fluxes from the set of 26 SMAP Core Validation Site towers. The L4_C V8 product continues to perform within specified accuracy requirements (Jones et al. 2017), with unbiased root-mean squared error (ubRMSE) in mean daily NEE well below 1.6 g C m^{-2} day^{-1} and a decrease in the ubRMSE for all fluxes relative to V7 (Figure 1). The V8 product shows stable performance for other metrics, albeit with a slight increase in bias and RMSE, and a decrease in spatially-averaged time series correlations (Table 1) relative to V7 for NEE, GPP, and RECO.

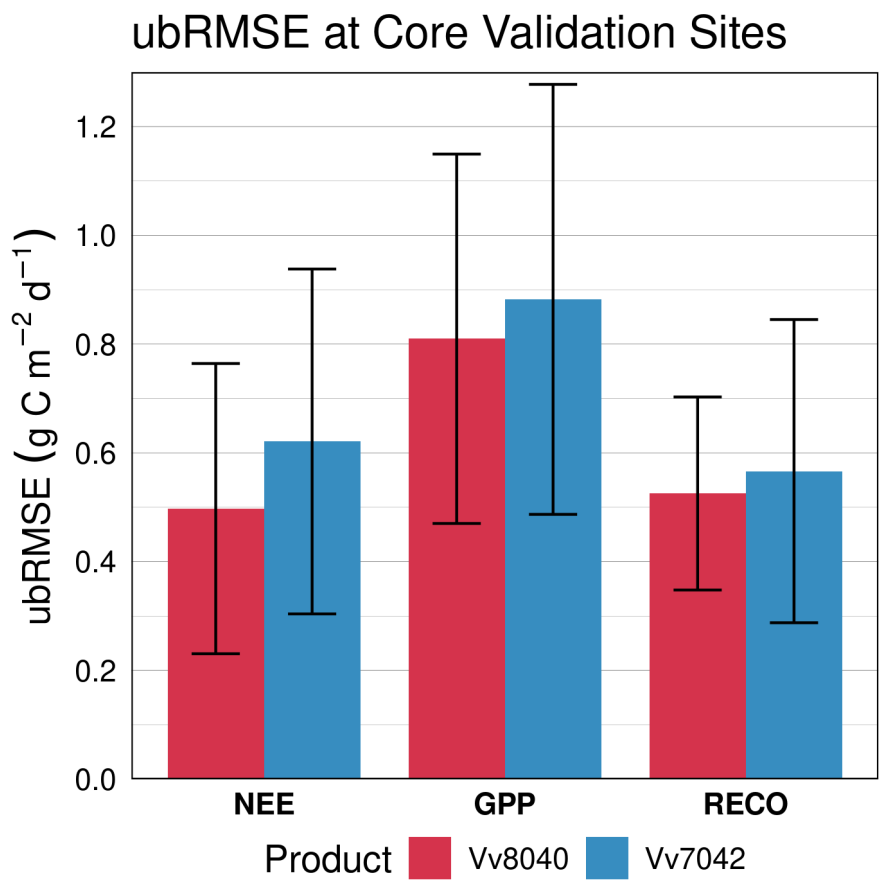

Figure 1: Unbiased root-mean squared error (ubRMSE) in NEE, GPP, and RECO for the L4_C V8 and V7 products, evaluated at the 26 Core Validation Sites.

Table 1: Mean bias, root-mean squared error (RMSE), and correlation for L4_C V7 and V8, evaluated at the Core Validation Sites. Bias and RMSE are in units of g C m^{-2} day^{-1}. Correlation is dimensionless.

Flux	Bias (V7)	Bias (V8)	RMSE (V7)	RMSE (V8)	Correlation (V7)	Correlation (V8)
NEE	0.27	0.30	0.98	0.96	0.62	0.55
GPP	0.30	0.31	1.32	1.35	0.76	0.71
RECO	0.66	0.73	1.16	1.16	0.69	0.68

As the SMAP mission has just completed its first decade of measurements, an assessment of recent performance should also consider the performance of the product versions over the full mission period. Over the past 10 years of record, NEE ubRMSE has improved steadily (Figure 2), including punctuated, substantial improvements in Version 3 and again in the most recent version.

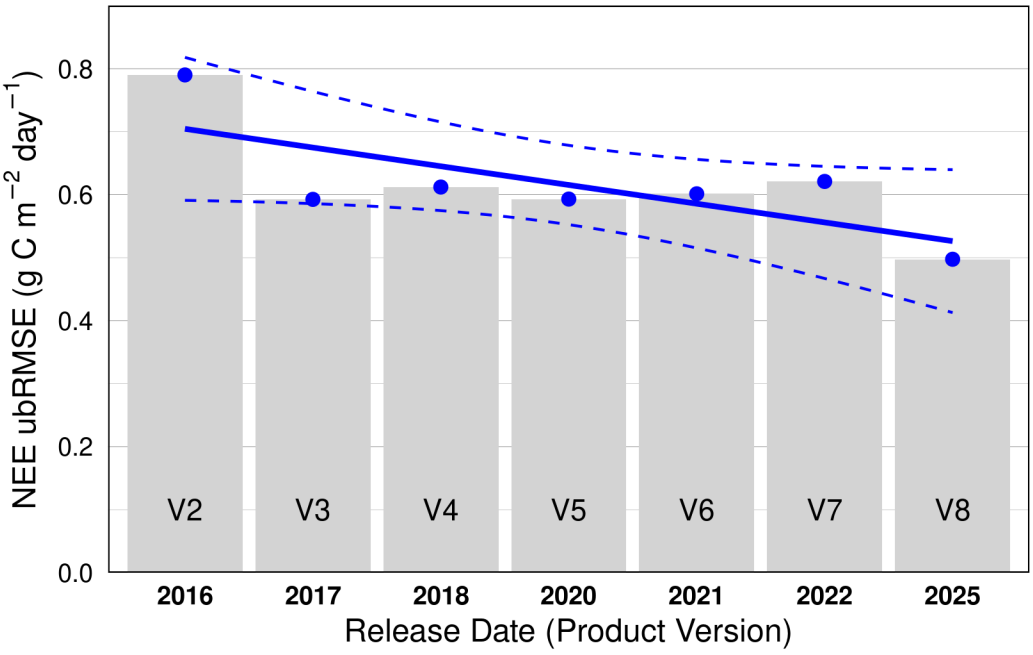

Figure 2: L4_C performance in estimating net ecosystem exchange (NEE) at the Core Validation Sites over successive product versions, in terms of unbiased root-mean squared error (ubRMSE), with a linear trend line shown. The validation period for V2 is 31 March – 31 December 2015, as reported in Jones et al. (2017). The validation period for V3-V8 is 31 March 2015 – 31 December 2017.

4 L4_C Product Comparisons Against Independent Data

In this section, we assess the performance of the L4_C V8 product against additional independent reference data sets.

4.1 Mean and Interannual Variability

Following the approach of a recent validation of the MODIS MOD17 productivity model (Endsley et al. 2023a), we compared L4_C V8 mean annual productivity (2016-2024) to alternative assessments in the literature. Mean annual GPP and NPP in L4_C V8 compare well (Figure 3) with both inter-model comparisons (Anav et al. 2015) and the broader literature (Cramer et al. 2001).

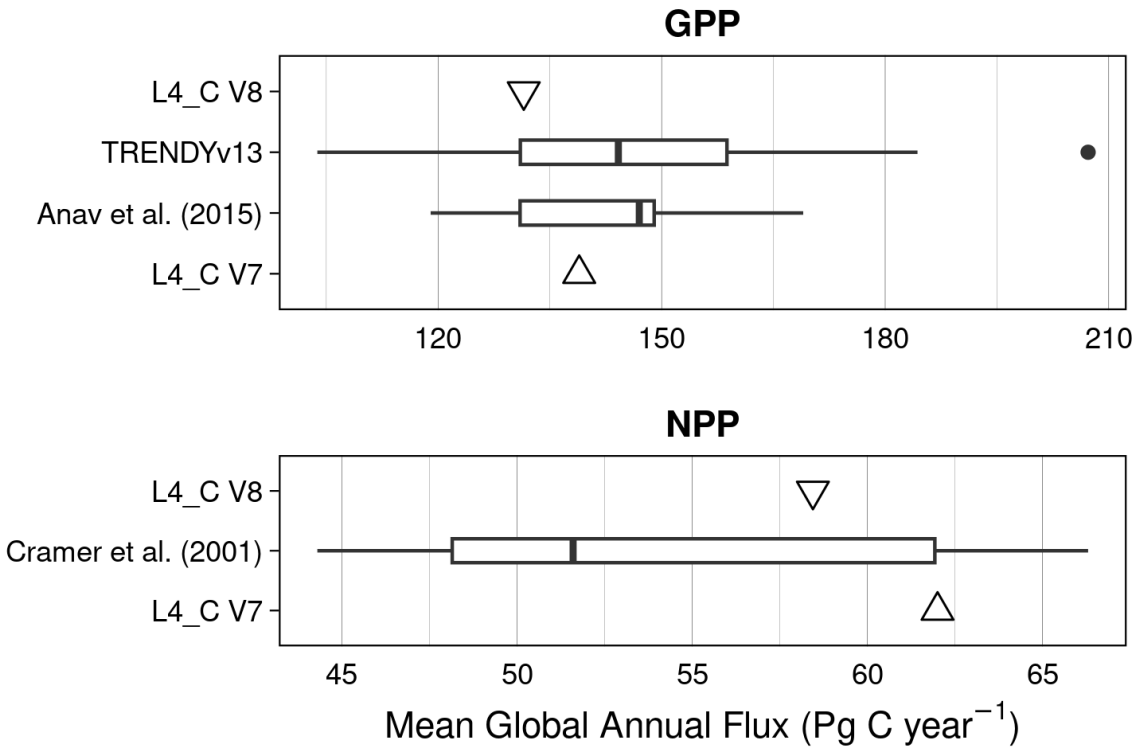

Figure 3: Comparison of L4_C V8 and V7 mean annual GPP and NPP (2016-2020) with independent estimates from model inter-comparisons (Anav et al. 2015 and the TRENDYv13 model ensemble) and the literature (Cramer et al. 2001). For TRENDYv13, we took the median annual flux for each model, for the years 2016-2023. The estimates of Anav et al. represent the period 1990-2009. The estimates from Cramer et al. 2001 represent a wide range of the 20th century, as they are compiled from multiple field studies. The box plots show the median, interquartile range, minimum, and maximum.

L4_C V8 also compares well with MODIS MOD17 (Collection 7) for the overlapping period of record, 2016-2021 (not shown): mean annual GPP in L4_C V8 is

131.6 (with interannual standard deviation of ± 1.6) Pg C $year^{-1}$, compared to 131.1 (± 0.9) Pg C $year^{-1}$ in MOD17. For mean annual NPP, L4_C V8 predicts 58.5 (± 0.7) Pg C $year^{-1}$, which is quite close to the MOD17 estimate of 58.9 (± 0.9) Pg C $year^{-1}$. This agreement is unsurprising, as both products use very similar GPP models. However, it is worth noting that L4_C V8 achieves a very similar NPP estimate using a less-sophisticated NPP model, while L4_C V8 also demonstrates higher interannual variability (IAV) in GPP, likely because it is sensitive to a wider range of environmental constraints, including soil moisture.

We also compared L4_C V7 and V8 to a recent global extrapolation of EC tower data, FLUXCOM-X (Nelson et al. 2024). We obtained 0.05-degree, equirectangular gridded estimates for FLUXCOM-X, a machine-learning extrapolation of EC tower data. The FLUXCOM-X estimates were resampled onto the 9-km global EASE-Grid 2.0 (Brodzik et al. 2012) of the L4_C product, using nearest-neighbor resampling, then aggregated by hemisphere and TransCom regions (Baker et al. 2006). Comparison with matching latitude-band summaries from FLUXCOM-X (2015-2020) indicate that L4_C V7 and V8 both adequately represent the IAV in RECO, GPP, and NEE in the Northern and Southern Hemisphere mid-latitudes and high latitudes (Figure 4). Flux IAV in the Tropics is so low that it makes for a difficult comparison. L4_C V8 shows clear improvement for RECO and mixed results for NEE in the Northern Hemisphere, where late-fall and winter respiration is reduced, relative to V7. Moreover, the overall amplitude of the northern terrestrial C sink is reduced compared to FLUXCOM-X and L4_C V7.

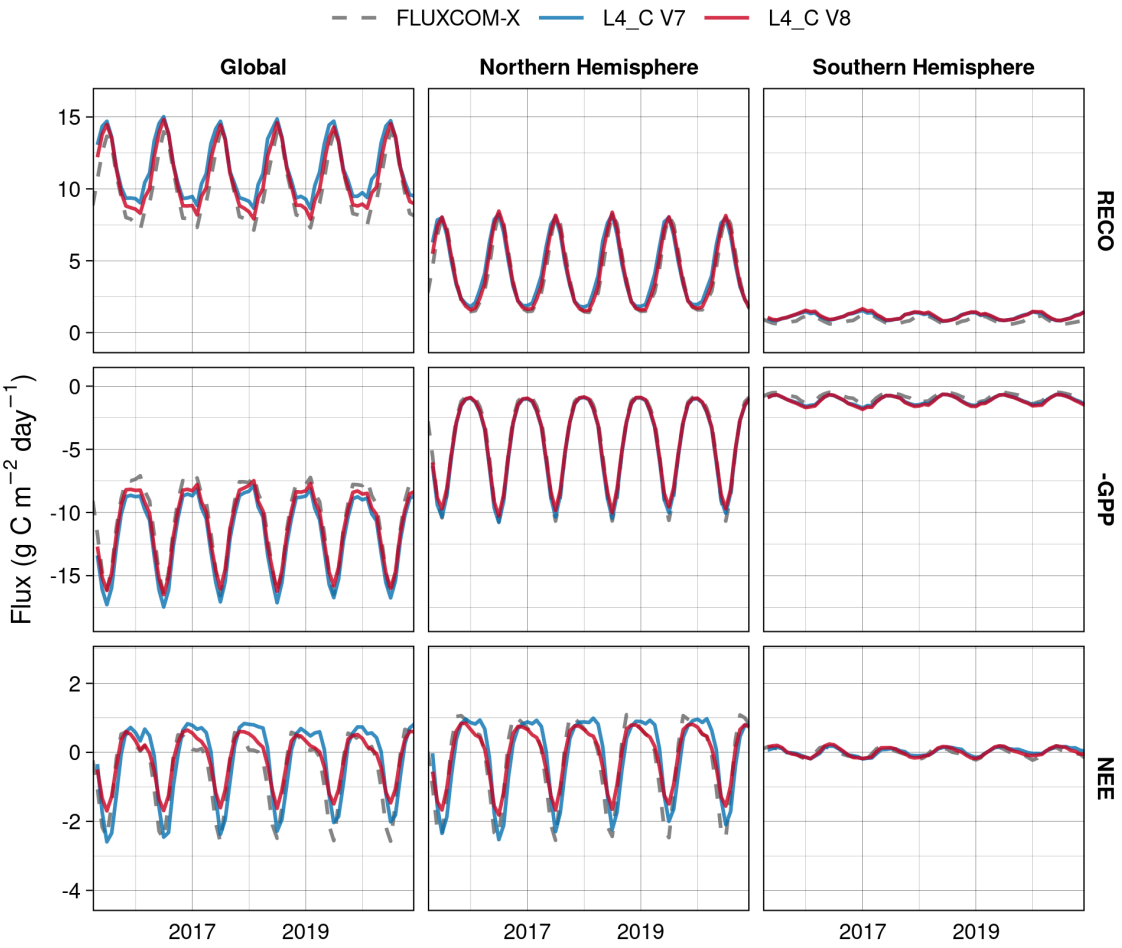

Figure 4: Mean daily RECO, GPP, and NEE from FLUXCOM-X and L4_C (V7 and V8) for the Global domain (90°S - 90°N latitude), the Northern Hemisphere (20-90°N latitude), and the Southern Hemisphere (20-90°S latitude). Note that the negative of GPP is plotted, for consistency with the definition NEE = RECO – GPP.

Monthly NEE anomalies from L4_C (both versions) compare well with FLUXCOM-X in all TransCom regions and especially well in the Northern Hemisphere TransCom regions (Figure 5). Notably, in the Boreal and Temperate regions, L4_C V8 shows a better match with FLUXCOM-X than does L4_C V7, apparently due to decreased fall respiration. In the Southern Hemisphere TransCom regions, L4_C V8 shows less seasonal bias than L4_C V7, evaluated against FLUXCOM-X (Figure 5). In terms of correlation, the L4_C V8 anomalies show generally improved agreement with FLUXCOM-X compared to that of V7 (Table 2).

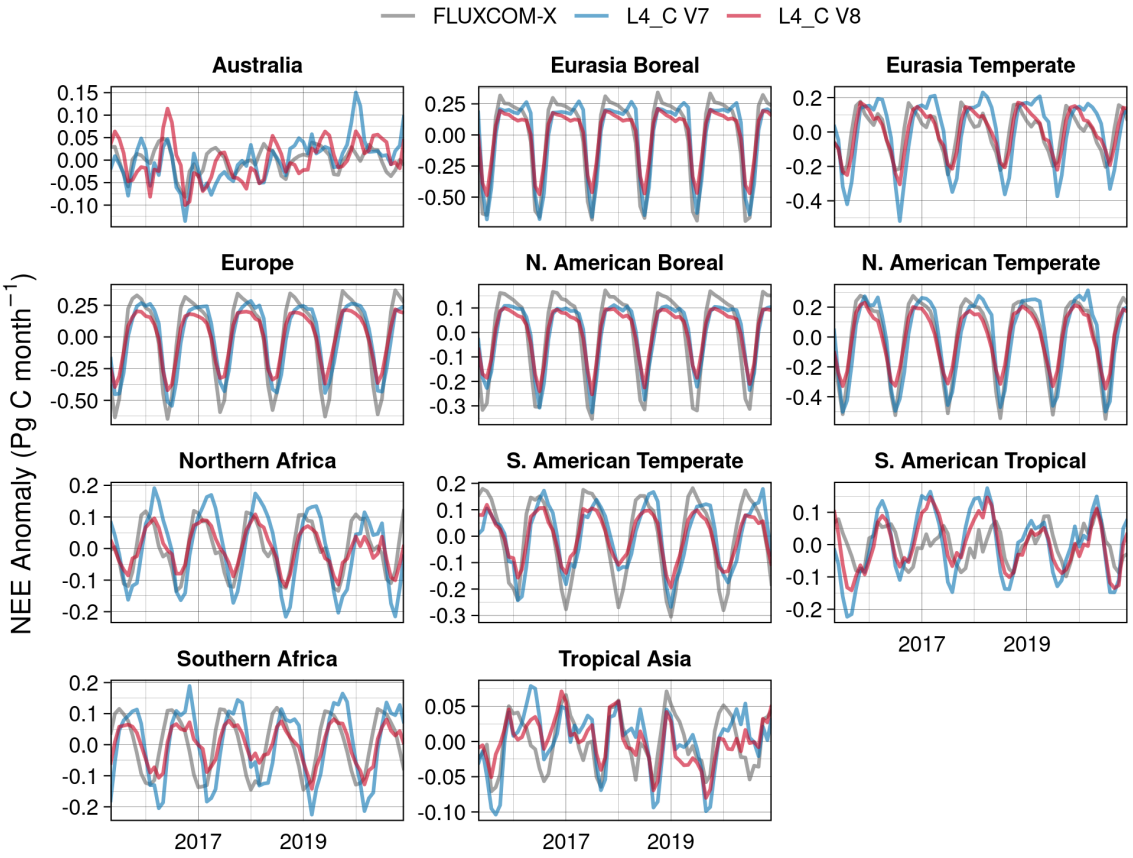

Figure 5: Monthly NEE anomalies for L4_C (V7 and V8) and FLUXCOM-X, for the period March 2015 through December 2020 and the TransCom regions.

Table 2: Pearson's correlation coefficients, expressing the degree of agreement between monthly NEE anomalies (2015-2020) from FLUXCOM-X and each L4_C version.

Region	L4_C V7	L4_C V8
Australia	0.454	0.442
Eurasia Boreal	0.923	**0.989**
Eurasia Temperate	0.629	**0.869**
Europe	0.903	**0.986**
N. American Boreal	0.914	**0.970**
N. American Temperate	0.911	**0.988**
Northern Africa	0.702	**0.849**
S. American Temperate	0.816	**0.960**
S. American Tropical	0.419	**0.590**
Southern Africa	0.416	**0.672**
Tropical Asia	0.618	**0.658**

Anomalies in annual fluxes reveal a correspondence between flux IAV and climatic extremes (Figure 6). For example, Australia's intense heat and drought in 2019 resulted in a sharp decline in both annual GPP and R_H (Endsley et al. 2023a). In Northern Africa, rainfall deficits in late 2016 through 2017 are also associated with declines in GPP (iSciences 2016), while in that same period, in Europe, the most severe drought since 1979 (García-Herrera et al. 2019) is associated with a sharp decline in GPP in 2017. To examine whether these anomalies may also be associated with climate oscillations, we compared annual flux anomalies with the outgoing long-wave radiation (OLR) index (Chiodi and Harrison 2013), a measure of the strength of the El Niño Southern Oscillation (ENSO) and its El Niño and La Niña phases (Figure 6). We find that in the Tropics (South American Tropical and Tropical Asia regions), R_H anomalies are correlated with the La Niña phase, which generally brings wetter conditions to these same regions (Holmgren et al. 2001; Bastos et al. 2018; Zhang et al. 2019) and would, therefore, increase R_H flux in those years.

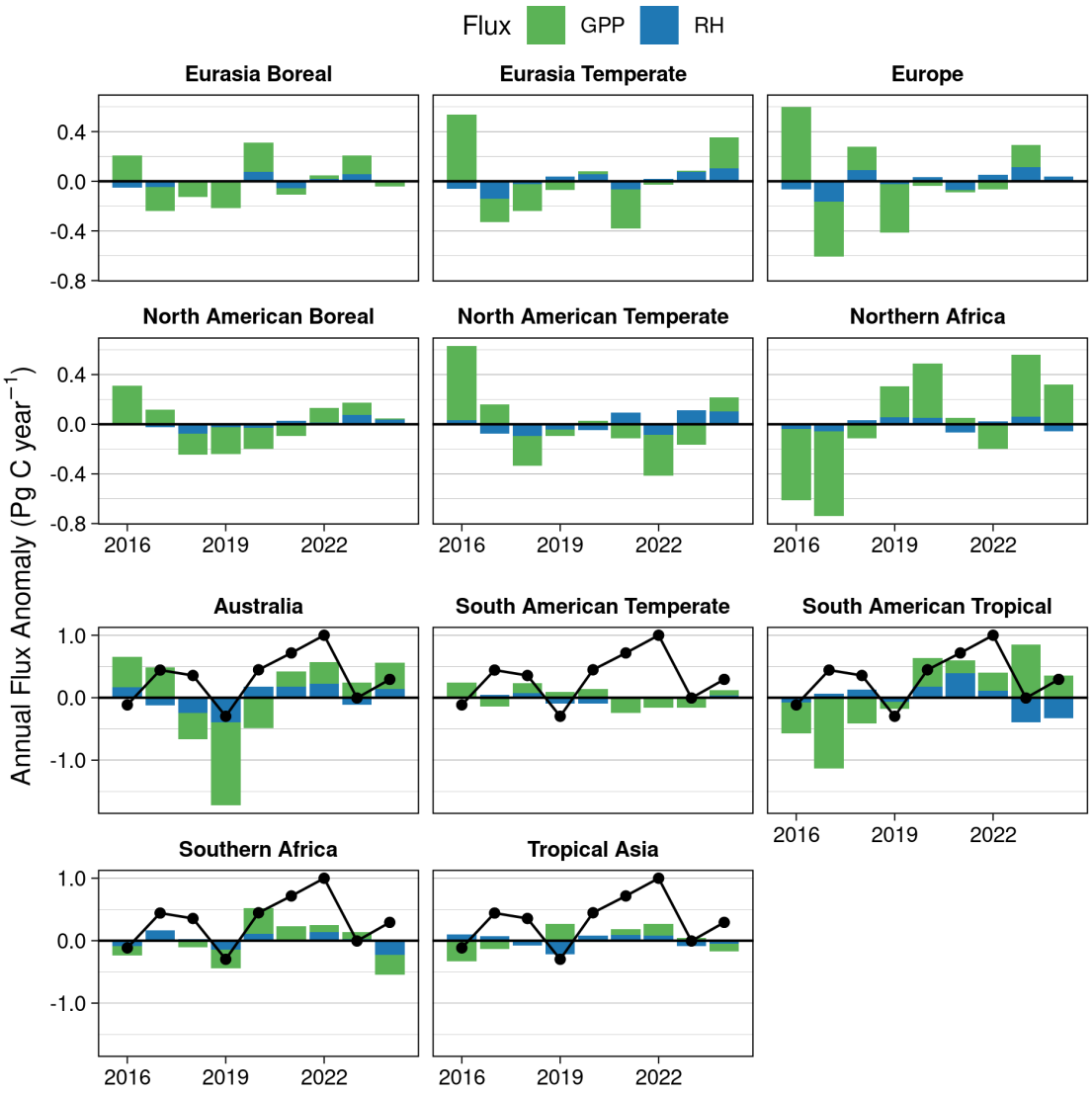

Figure 6: Annual R_H and GPP anomalies for L4_C V8, shown for each TransCom region. For regions in the Tropics and the Southern Hemisphere, the outgoing long-wave radiation (OLR) index is super-imposed as a black line.

4.2 Seasonal Cycle of Ecosystem Respiration

One of the major algorithm improvements to L4_C V8 is the addition of a seasonally varying litterfall phenology, which is expected to correct a bias in the seasonal cycle of RECO and NEE (Endsley et al. 2022). We also compared L4_C flux estimates to monthly, global and regional means from FLUXCOM-X and another product, the TRENDY version 13 (TRENDYv13) ensemble (Sitch et al. 2024). These ensembles are expected to provide a good representation of the annual RECO cycle because they pool multiple (physical or data-driven) model estimates together. In particular, FLUXCOM-X is an empirical and globally contiguous up-scaling of EC tower data.

TRENDYv13 is a collection of estimates from 21 dynamic global vegetation models. We chose to use data from the "S3" simulation, which includes varying atmospheric CO_2, climate, and land use scenarios. One of the models was excluded because the time coordinates could not be deciphered. We resampled each model's monthly GPP and NEE estimates onto a half-degree equirectangular grid, the finest grid spacing of any of the models, using nearest-neighbor resampling. GPP was available for every model. When NEE was not available in the model's output, it was computed either from net ecosystem productivity (NEP, the additive inverse of NEE) or by subtracting GPP from the sum of R_H and R_A, depending on what data were available for that model. Fluxes were then converted from [kg C $m^{-2}sec^{-1}$] to [g C $m^{-2}month^{-1}$]. To calculate regional and global totals, the half-degree estimates were resampled on an equal-area grid, the 36-km global EASE-Grid 2.0, using nearest-neighbor resampling.

When we compare L4_C RECO and NEE to FLUXCOM-X or TRENDYv13 (ensemble mean) by latitude band, we find that L4_C V8 has substantially improved the seasonal cycle of both fluxes (Figure 7). In the Northern Hemisphere mid- and high latitudes (>20°N latitude), the seasonal cycle of RECO in L4_C V8 is shifted slightly forward in time (relative to V7), with peak RECO occurring 1-2 weeks later in the year, which is more consistent with the RECO cycle depicted by both FLUXCOM-X and TRENDYv13. This gives rise to a seasonal cycle of NEE that is shifted backward in time, with peak sink activity occurring ca. 2 weeks earlier in the year. The backward shift in NEE is of a greater magnitude due to the differencing between GPP and RECO. It's interesting that this effect is also seen in the Southern Hemisphere (<20°S), given that the smaller land domain and different PFT composition result in generally less pronounced leaf phenology. In the Tropics (between 20°S and 20°N), L4_C is less accurate in representing the seasonal cycle, likely because of the very low characteristic seasonality in tropical leaf phenology, at least in terms of satellite-observed fPAR.

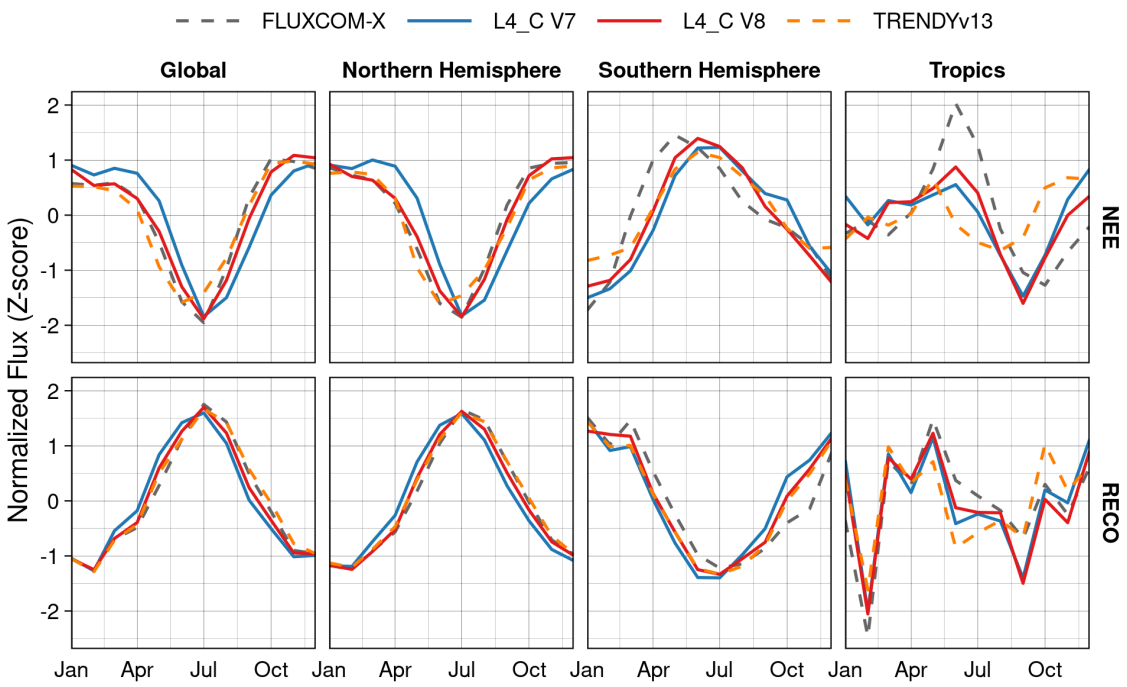

Figure 7: Normalized seasonal cycle of NEE and RECO (2015-2020) for FLUXCOM-X, L4_C (V7 and V8), and the TRENDYv13 ensemble mean for the Global domain (90°S - 90°N latitude), the Northern Hemisphere (20-90°N latitude), the Southern Hemisphere (20-90°S latitude), and the Tropics (20°S - 20°N latitude).

The L4_C V8 seasonal cycle of NEE aligns better with FLUXCOM-X than with TRENDYv13 and, indeed, we would expect FLUXCOM-X to be a more faithful representation because it upscales tower-measured fluxes and is validated against atmospheric CO_2 data. As such, we looked in detail at the differences between the seasonal cycles of L4_C and FLUXCOM-X. For regions north of the Equator, a spring high bias and fall low bias in L4_C V7 RECO were both substantially reduced in V8 (Figure 8), almost certainly because the new litterfall scheme shifted the seasonal allocation of litter to SOC pools. However, in Northern Africa, seasonal RECO bias is not improved although it is improved for NEE (Figure 9), suggesting that changes in GPP also contribute to the modified seasonal cycle of NEE in L4_C V8.

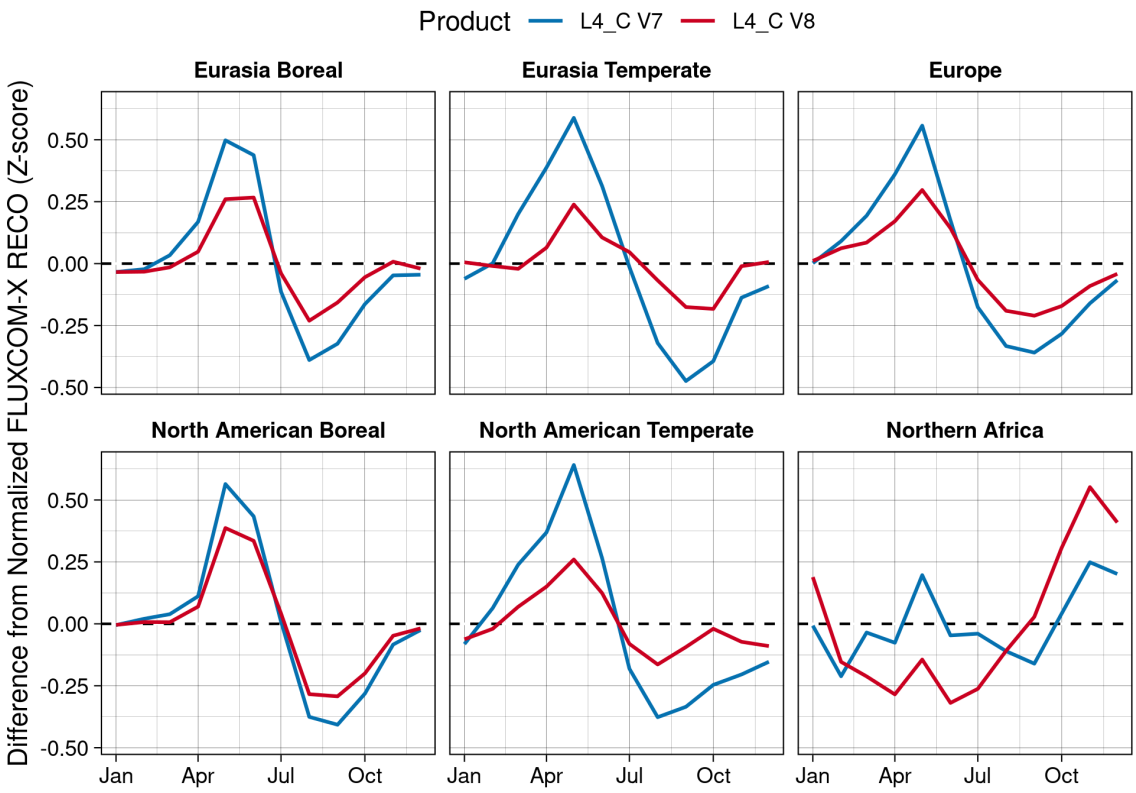

Figure 8: Difference in the monthly seasonal RECO cycles of L4_C and FLUXCOM-X (2015-2020). After computing the RECO seasonal cycle for each product, at monthly time steps, L4_C estimates (for V7 and V8) are subtracted from that of FLUXCOM-X.

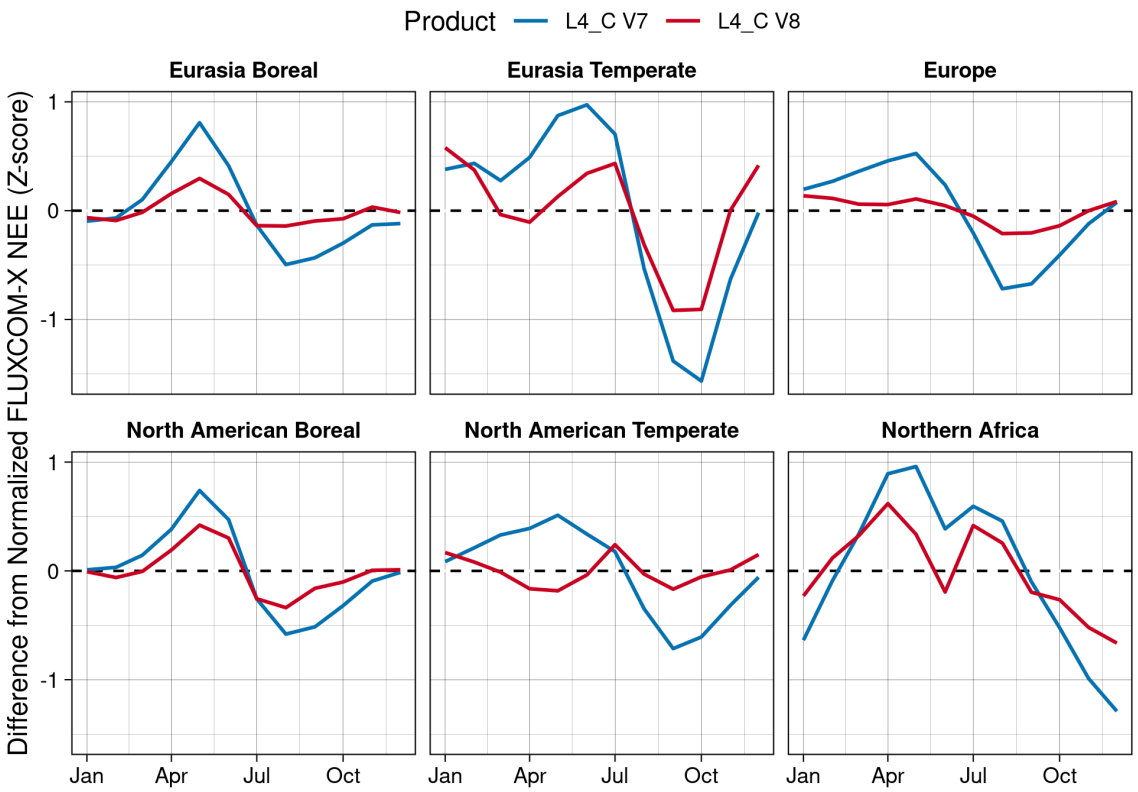

Figure 9: As in Fig. 8 but for NEE.

4.3 Gross Primary Productivity and Solar-Induced Fluorescence

The L4_C V8 seasonal cycle of GPP was compared to satellite-based, solar-induced chlorophyll fluorescence (SIF), which is a good proxy for photosynthetic activity. As in the V7 product assessment, global, spatially contiguous SIF (CSIF) data based on Orbiting Carbon Observatory-2 (OCO-2) retrievals, available at 0.05-degree resolution on 4-day intervals (Zhang et al. 2018), were resampled onto the global 9-km EASE-Grid 2.0, summarized by TransCom region, and converted to Z-scores for the SMAP post-launch period through the end of 2020. Throughout the Northern Hemisphere, L4_C V8 shows strong correlations with SIF ($r \geq 0.97$) and correlates well everywhere else, except in Northern Africa ($r = -0.153$) and the South American Tropics ($r = 0.058$) (Figure 10).

The performance of L4_C V8 GPP in Australia is particularly good, given that this region, more than any other, demonstrates strong inter-annual variability in photosynthetic activity (Figure 10). L4_C V8 GPP matches the relative magnitudes of CSIF in each year, with dry years (2019) showing both lower GPP and CSIF than wet years (2017). The poor correspondence in Northern Africa is due to an apparent phase shift in the seasonal cycle of L4_C GPP relative to that of SIF. Seasonal variability in L4_C GPP is largely driven by variability in fPAR, which may not be a good signal of photosynthetic activity in this very dry region. In the South American Tropical region, a

similar phase shift is evident, with overall greater noise in the L4_C GPP seasonal cycle, which may reflect the saturation of fPAR in closed-canopy, tropical forests. L4_C GPP also does not capture the twice-annual peak in photosynthetic activity evident from the SIF data in the South American Tropical region, although it does demonstrate this pattern in Southern Africa (Figure 10).

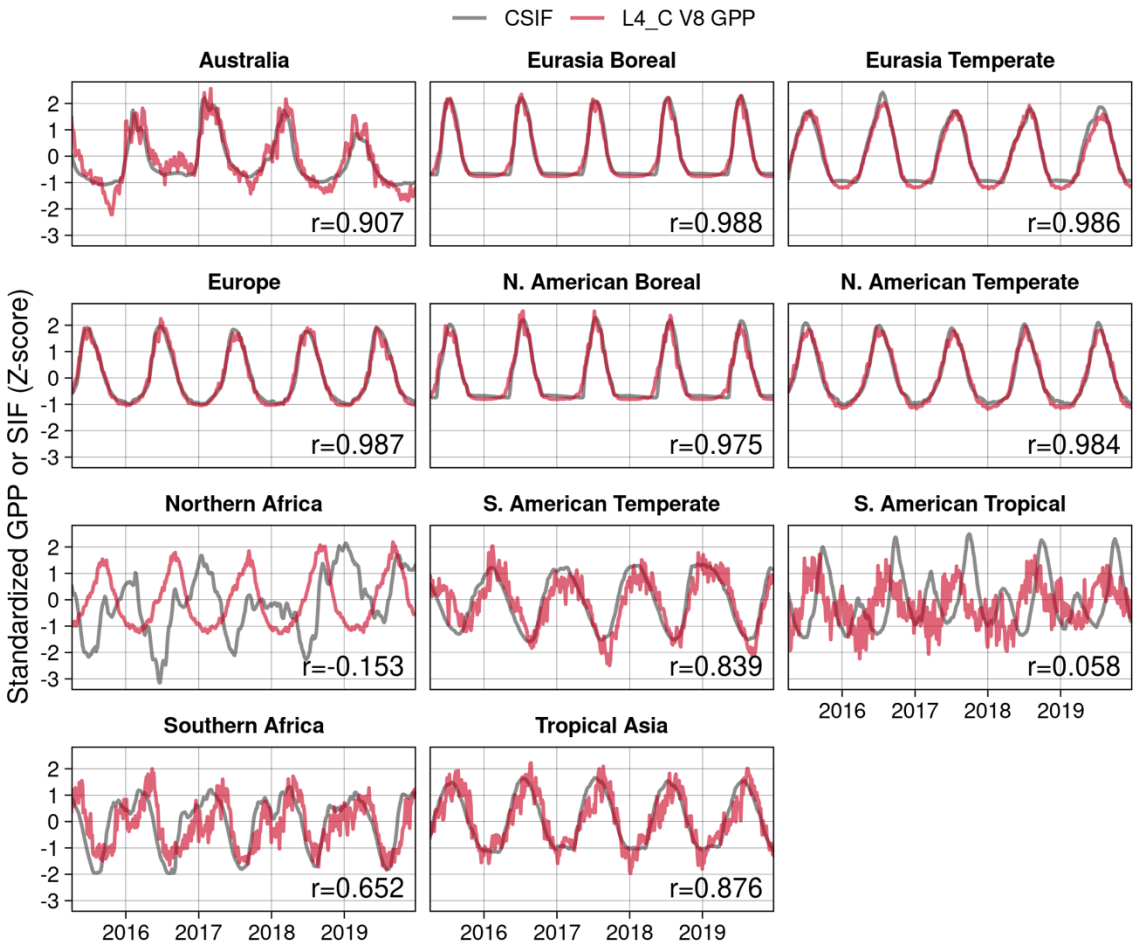

Figure 10: Standardized L4_C V8 GPP time series (i.e., converted to Z-scores) shown with standardized, contiguous solar-induced fluorescence (CSIF) data, for each TransCom region, at 4-day time steps. The Pearson's correlation is shown in the bottom-right corner of each plot.

It is notable that L4_C GPP has slightly lower correlations with CSIF in V8 than in V7 [compare Figure 10 to Figure 13 of (Endsley et al. 2023b)]. In Southern Africa, the correlation is considerably lower ($r = 0.65$ in V8 versus $r = 0.84$ in V7), which is almost certainly due to the change in VPD and Tmin parameters for the Shrubland (SHB) and Grassland (GRS) PFTs, perhaps leading to less sensitivity in L4_C GPP to environmental constraints in this region. However, L4_C V8 displays a more prominent semi-annual GPP cycle in Southern Africa than does V7, which is more consistent with CSIF data in the region (not shown).

Whereas the OCO-2 CSIF data used here is available only through the end of 2019, a new SIF proxy has recently become available (Fang et al. 2025), extending the temporal record of these kinds of measurements. The Long-term Continuous SIF-informed Photosynthesis Proxy (LCSPP) dataset provides a "SIF-informed, long-term photosynthesis proxy" based on remotely sensed surface reflectance data from MODIS. Based on this monthly record, L4_C GPP in V8 compares very well with the seasonal cycle of productivity, with long-term (2015-2023) correlations in most regions ≥ 0.8 (Figure 11).

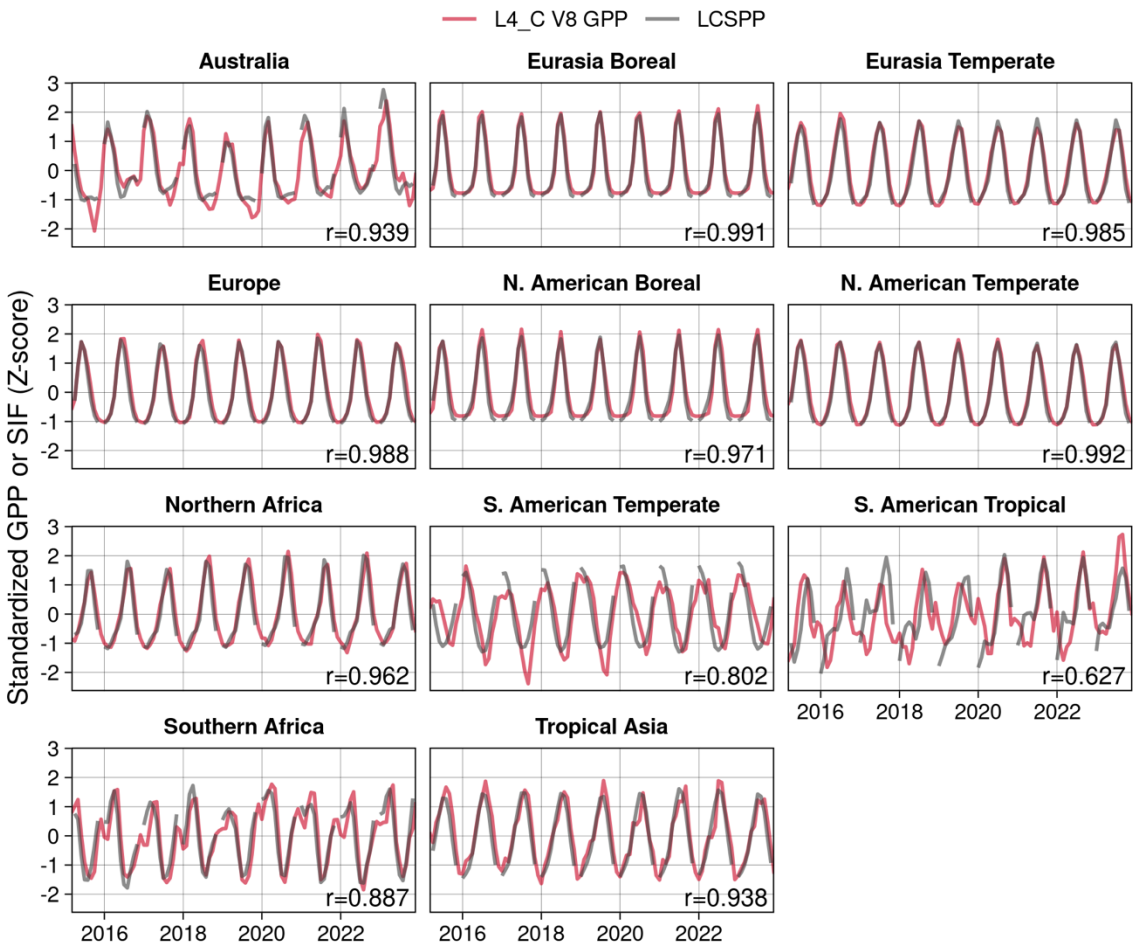

Figure 11: As in Fig. 10 but for monthly records and using the LCSPP index as a proxy for SIF.

4.4 Mean Surface Soil Organic Carbon Stocks

The new SOC calibration data are suggestive of a larger SOC stock than in previous versions. This was evident early in the V8 re-processing, when steady-state estimates based on the L4_SM Nature Run version 11.4 (NRv11.4) were compared to the previous, V7 post-calibration estimates, Nature Run version 10 (NRv10). When comparing these two post-calibration, steady-state SOC estimates to the SoilGrids 250m dataset (Hengl et

al. 2017), for multiple depths, we find that the V8 estimates are consistently larger than those from the previous version (Figure 12). Since Version 4, the L4_C estimates have been thought to represent an effective soil depth of ~5 cm (Endsley et al. 2020), consistent with the effective penetration depth of the L-band radiometer. But the comparison of L4_C V8 (based on NRv11.4) with data from the SoilGrids 250m product suggests that the L4_C V8 SOC estimates are representative of a deeper soil horizon, based on the 1:1 line seen in Figure 12.

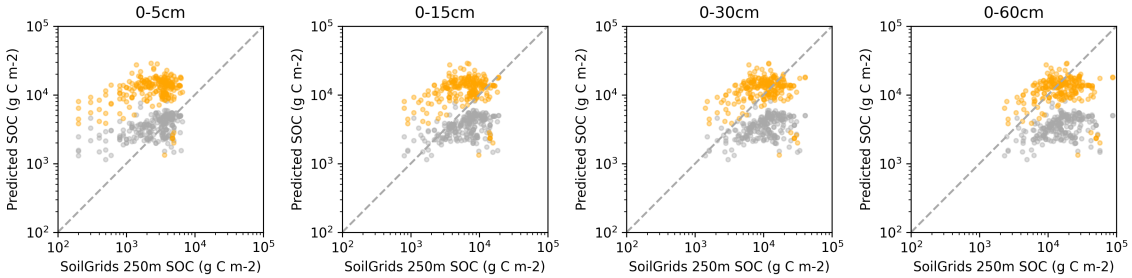

Figure 12: L4_C predicted soil organic carbon (SOC) content, at calibration sites, compared with the prediction of the SoilGrids 250m product. The L4_C Nature Run products are shown, with Nature Run version 10 (NRv10) shown as gray dots and the new, Nature Run version 11.4 (NRv11.4) shown in orange dots. NRv10 and NRv11.4 are multi-decadal, model-only simulations used in the development of V7 and V8, respectively, of L4_SM and L4_C.

However, the multiple changes to the SOC model in L4_C V8 seem to require a different approach to SOC spin-up, going forward. We could not obtain SOC pools in the quasi-equilibrium state during calibration, as in previous versions. Indeed, numerical spin-up performed for 1000 years (100 times longer than in previous versions) still did not lead to global convergence. Instead, the post-launch SOC states from 31 March 2025 were used to re-initialize a new forward run (leading to a minor version upgrade from Science Version ID Vv8020 to Vv8040). The post-launch SOC pools are in the quasi-equilibrium state and slightly smaller than the post-calibration, NRv11.4 SOC data, yet still indicative of a larger SOC stock than in V7 (and NRv10). A latitude-band comparison with SoilGrids 250m and the TRENDYv13 ensemble indicates that the new L4_C V8 SOC stock is more similar to a 15-cm soil horizon (Figure 13), although L4_C continues to under-estimate SOC storage at high latitudes and over-estimate storage in the southern tropics.

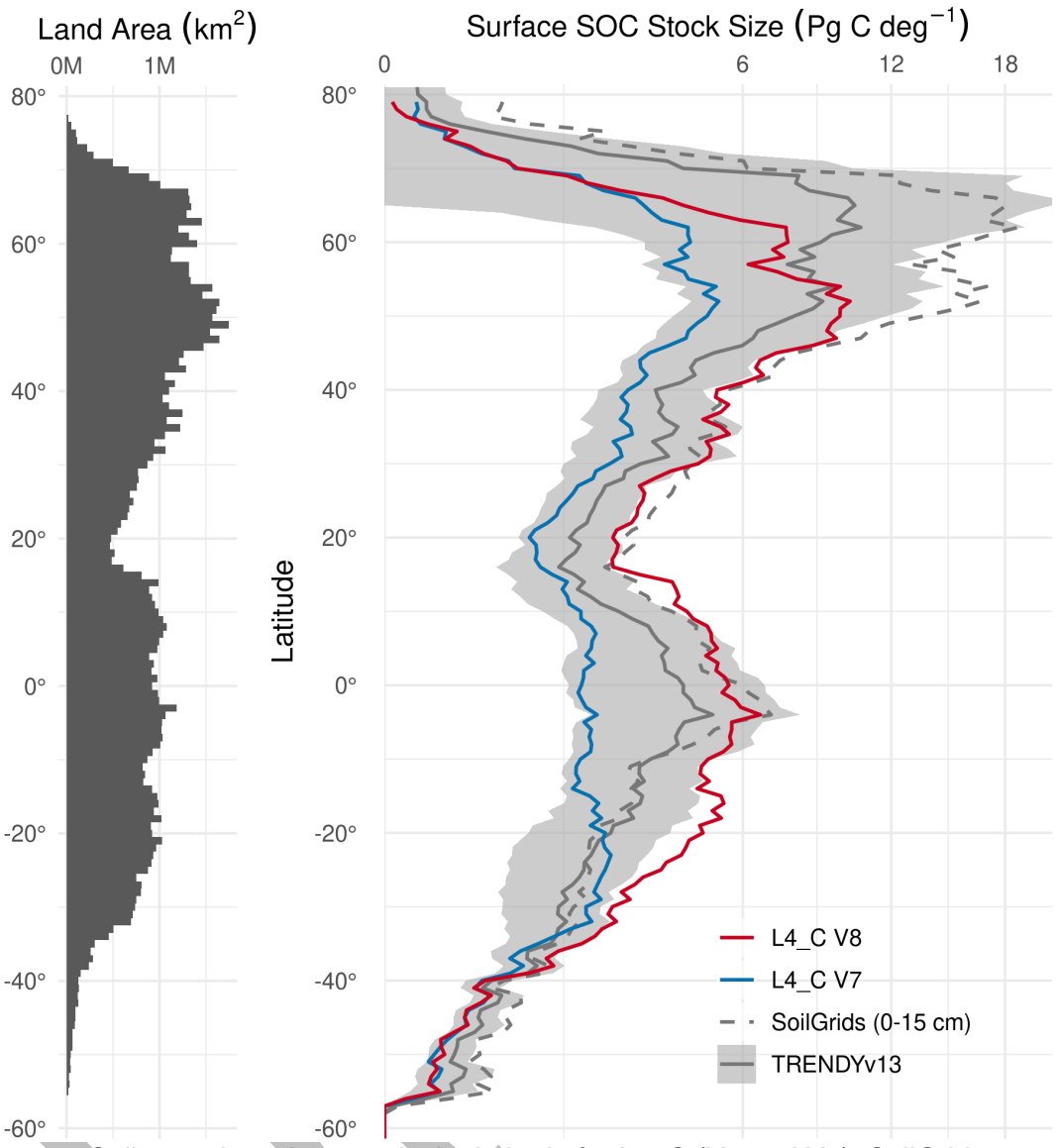

Figure 13: Soil organic carbon stocks by latitude for L4_C (V7 and V8), SoilGrids 250m, and TRENDYv13. The SoilGrids 250m product is vertically resolved, so the first two layers (0-5 cm, 5-15 cm) are shown totaled. The TRENDYv13 ensemble mean (solid gray line) is shown with one, inter-model standard deviation (shaded area).

4.5 Variability in Surface Soil Organic Carbon

As noted in previous assessments of L4_C, one thing that distinguishes the product from similar, global, gridded ecosystem-level estimates is that L4_C predicts daily SOC content. While SOC stocks do indeed vary on sub-annual time scales (Cagnarini et al. 2019; Padarian et al. 2022), it is generally not possible to validate dynamic SOC estimates, as field-based methods are destructive. Nonetheless, SOC changes in L4_C essentially function as a record of the accumulated changes in NEE and may contain a signal of ecosystem responses to short-term climate variability (Endsley et al. 2020).

We computed detrended SOC residuals from a harmonic regression, removing the seasonal cycle from the SOC time series for each TransCom region (Figure 14). The patterns are largely similar to those seen in the previous assessment report (Endsley et al. 2023b), in which we observed that SOC variability in most regions is completely described by a predictable annual cycle. There are, as in L4_C V7, a few notable exceptions, In Australia, we again observe a build-up in SOC content as the continent experiences the steepest drought (in 2019) since 1900 (*ibid.*). Starting in 2020, the continent experienced normal rainfall levels and even regional pluvial events in 2022 and 2024 (Australia Bureau of Meteorology 2024), which coincide with a gradual reduction in SOC content.

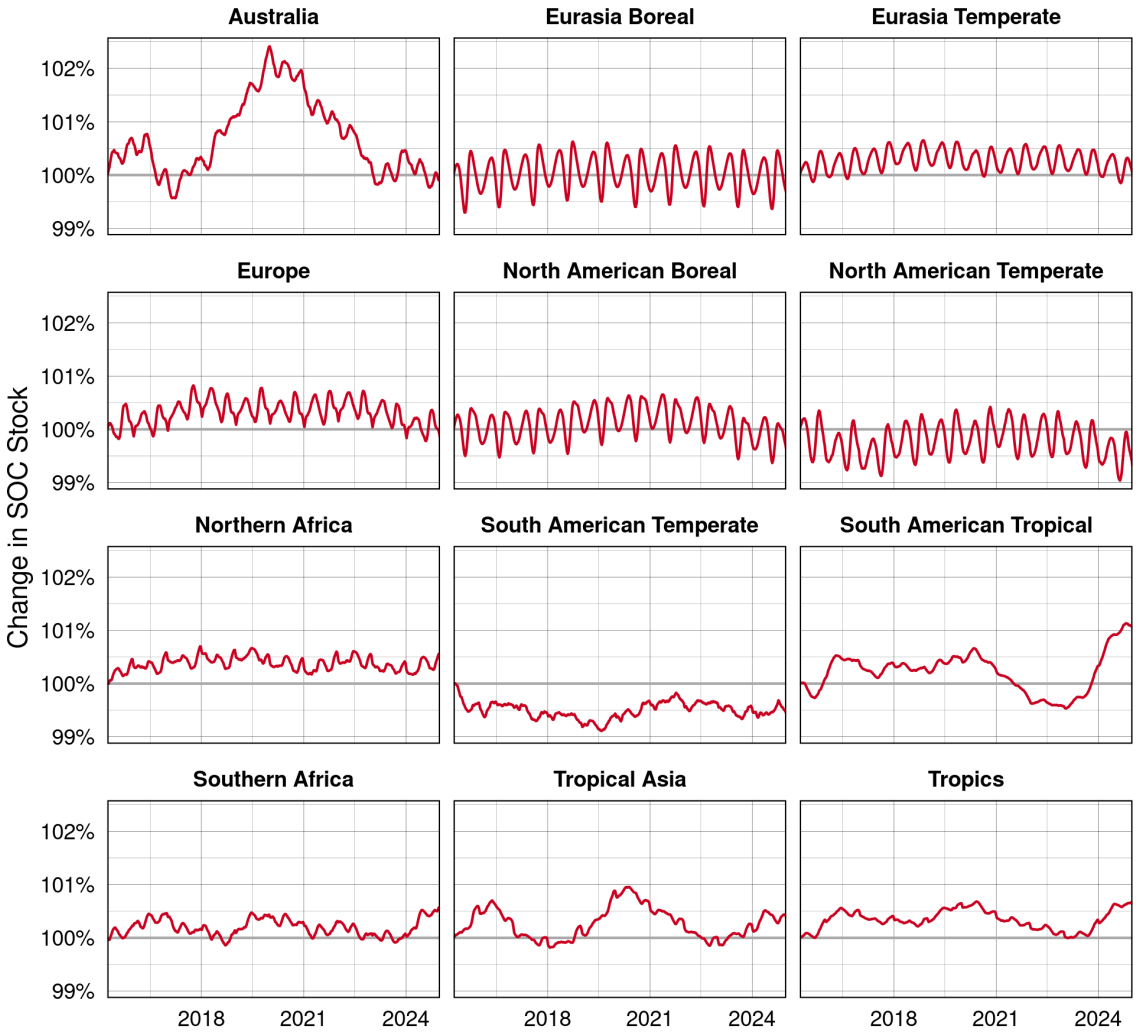

Figure 14: Detrended anomalies in L4_C V8 soil organic carbon (SOC) content, from harmonic regression, by TransCom region. The vertical axis expresses percent change in SOC stock since March 31, 2015, the start of the record.

Residual SOC dynamics are also observed in Southern Africa and the tropical regions. In these regions, residual SOC change is correlated with the El Niño Southern Oscillation (ENSO) (Figure 15), based on the outgoing long-wave radiation (OLR) index (Chiodi and Harrison 2013), a measure of the strength of this global climate oscillation and the corresponding El Niño and La Niña phases. We find that a 9-month leading OLR index shows moderately strong correlations ($r \geq 0.5$) with residual SOC change. This finding is consistent with the regional climate responses to El Niño (La Niña), which is associated with anomalously dry (wet) conditions in these same regions (Holmgren et al. 2001; Bastos et al. 2018; Zhang et al. 2019). Similar to the build-up of residual SOC in Australia in 2019, a sharp increase in residual SOC content in the South American Tropical region through 2024 coincides with deep drought in the Amazon basin, despite the mild La Niña conditions. Although La Niña conditions are generally associated with a stronger land C sink in tropical drylands (Ahlström et al. 2015), we should note that the impact of ENSO on residual SOC stocks is reversed, possibly because L4_C only perturbs SOC through changes in moisture and temperature, with NPP inputs to SOC being fixed based on the long-term average productivity of the ecosystem. Consequently, while these residual SOC changes illustrate the model's sensitivity to climate (see Endsley et al. 2023b for a more thorough analysis), the model lacks a dynamic connection to productive inputs (NPP), which are known to be lower during the El Niño phase (Hashimoto et al. 2004; Zhu et al. 2017; Bastos et al. 2018).

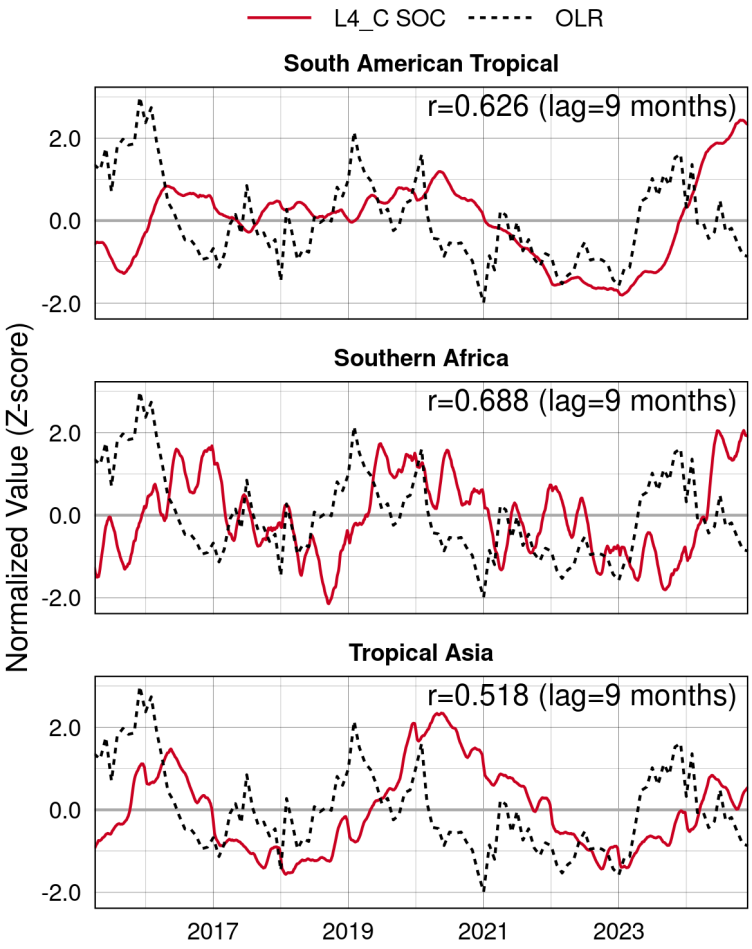

Figure 15: Residual L4_C V8 soil organic carbon (SOC) content (detrended anomalies from harmonic regression) and outgoing long-wave radiation (OLR) index. The sign of the OLR index is flipped so that positive (negative) values correspond to the El Niño (La Niña) phase. The maximum Pearson's correlation, from cross-correlation, is shown with the value of the corresponding lag.

5 Summary and Potential Future L4_C Product Updates

The multiple assessments described here indicate that the L4_C V8 product continues to provide a level of performance and accuracy consistent with the product's science objectives. Multiple changes were made to the product after V7, and the latest version (V8) demonstrates a significant increase in accuracy (reduction in ubRMSE) as well as much improved correlation with the seasonal RECO and NEE cycles predicted by independent models. These achievements make L4_C V8 a good candidate for integration with atmospheric modeling studies, potentially serving as a prior for atmospheric inversion, among other applications.

The new SOC model and litterfall mechanism in L4_C V8 have resulted in larger SOC stock sizes than those of previous versions. A comparison to the SoilGrids 250m product and the TRENDYv13 model ensemble indicate that L4_C V8 SOC provides a similar spatial pattern and is consistent with the SOC content in the top 15 cm of soil. Our comparison with satellite-based, solar-induced fluorescence data show that L4_C V8 GPP continues to represent well the seasonal cycle and variability of terrestrial productivity. L4_C V8 also shows very good correspondence with the monthly variability in NEE, GPP, and RECO predicted by the FLUXCOM-X global extrapolation, which indicates that the mechanistic, diagnostic model framework of L4_C is capable of reproducing the carbon fluxes predicted by a highly parameterized, machine-learning framework trained on EC tower data.

Future releases of the SMAP L4_C operational product will incorporate ongoing refinements and improvements to upstream inputs, including in the L4_SM algorithm. The recent changes (from V7 to V8) have revealed that further changes to L4_C model logic will be challenging, given the operational constraints and the legacy of the current algorithm code. We also note that we already implemented three of the four proposed changes from the previous L4_C product assessment. Nevertheless, the following changes to input datasets and model logic may be achievable:

- The changes to the SOC model have disrupted the normal spin-up procedure used in previous versions. We will need to evaluate both the assumptions about SOC decay coefficients as well as the approach to model spin-up in the next version. To adjust decay coefficients, we might try scaling our SOC calibration data using the same empirical, depth-decay coefficients that were used to compare L4_C SOC with alternative assessments in Endsley et al. (2020). To improve spin-up, we might use the previous version's SOC map as the initial SOC estimate rather than the analytical solution, which always under-estimates SOC storage.
- L4_C currently uses the long-term mean annual NPP to determine how much C input to allocate to SOC pools (over the course of a year). While the recent updates to the litterfall representation have improved the *timing* of this C allocation, the overall amount allocated is fixed, based on the long-term mean. An alternative would be allocate C based on some lagged, aggregated estimate of NPP, since L4_C

already computes this quantity. This would add realism by representing C limitation in the soil community, which could potentially improve the resulting R_H flux estimates and better represent interannual variability in carbon fluxes.

- The V8 change in litterfall allocation altered the global, spatial distribution of SOC stocks and their magnitudes. In some areas, this has resulted in less realistic SOC magnitudes. This may suggest that the assumption of a constant daily fraction of NPP may be necessary to improve SOC stock estimation in some areas. We should examine whether the pixel-wise allocation fractions should be fixed at 1/365 (i.e., even amount every day of the year) for some pixels.
- Despite the recent change to the *timing* of litterfall allocation, the L4_C algorithm still prescribes different *amounts* of litterfall (as a fraction of the allotted NPP) for each PFT to the two fastest SOC pools. This assumption should be re-examined.
- As suggested in the previous L4_C assessment, adding an upper limit on the response of R_H to soil moisture, in the form of a limitation on O_2 diffusion, could improve model realism and RECO performance when soils are close to saturation. As demonstrated in Endsley et al. (2022), some form of an O_2 diffusion limitation can improve the L4_C soil decomposition and R_H model. This could take the form of a second linear ramp function on the response of R_H to increasing soil moisture, or a Michaelis-Menten diffusion kinetics-type model.

Acknowledgements

Funding for this work was provided by the NASA Soil Moisture Active Passive (SMAP) mission. Computing resources were provided by the NASA Center for Climate Simulation (NCCS). This work used eddy covariance data acquired by the FLUXNET community, which was supported by the CarboEuropeIP, CSIRO, FAO-GTOS-TCO, iLEAPS, Max Planck Institute for Biogeochemistry, National Science Foundation, National Research Infrastructure for Australia, Terrestrial Ecosystem Research Network, University of Tuscia, Université Laval and Environment Canada, US Department of Energy and NOAA ESRL, as well as many local funders including the Global Change Research Centre AS Czech Republic, Wisconsin Focus on Energy, and Forest Department of the Autonomous Province of Bolzano – CO_2-measuring station of Renon/Ritten. Funding for the AmeriFlux data portal was provided by the U.S. Department of Energy Office of Science. We thank Drs. A.E. Andrews, M. Aurela, D. Baldocchi, J. Beringer, P. Bolstad, J. Cleverly, B.D. Cook, K.J. Davis, A.R. Desai, D. Eamus, E. Euskirchen, J. Goodrich, L. Hutley, A. Kalhori, H. Kwon, B. Law, C. Macfarlane, W. Oechel, S. Prober, K. Rautiainen, R. Scott, H. Wheater, D. Zona and many other PIs for sharing their flux tower data.

References

Ahlström, A., M. R. Raupach, G. Schurgers, B. Smith, A. Arneth, M. Jung, M. Reichstein, J. G. Canadell, P. Friedlingstein, A. K. Jain, E. Kato, B. Poulter, S. Sitch, B. D. Stocker, N. Viovy, Y. P. Wang, A. Wiltshire, S. Zaehle, and N. Zeng. 2015. The dominant role of semi-arid ecosystems in the trend and variability of the land CO2 sink. *Science* 348 (6237):895–899.

Anav, A., P. Friedlingstein, C. Beer, P. Ciais, A. Harper, C. Jones, G. Murray-Tortarolo, D. Papale, N. C. Parazoo, P. Peylin, S. Piao, S. Sitch, N. Viovy, A. Wiltshire, and M. Zhao. 2015. Spatiotemporal patterns of terrestrial gross primary production: A review. *Reviews of Geophysics* 53 (3):785–818.

Australia Bureau of Meteorology. 2024. Australian rainfall deciles since 1900. https://www.bom.gov.au/climate/history/rainfall/ (last accessed 12 August 2025).

Baker, D. F., R. M. Law, K. R. Gurney, P. Rayner, P. Peylin, A. S. Denning, P. Bousquet, L. Bruhwiler, Y. H. Chen, P. Ciais, I. Y. Fung, M. Heimann, J. John, T. Maki, S. Maksyutov, K. Masarie, M. Prather, B. Pak, S. Taguchi, and Z. Zhu. 2006. TransCom 3 inversion intercomparison: Impact of transport model errors on the interannual variability of regional CO2 fluxes, 1988-2003. *Global Biogeochemical Cycles* 20 (1), GB1002, doi:10.1029/2004GB002439.

Baldocchi, D. 2008. 'Breathing' of the terrestrial biosphere: Lessons learned from a global network of carbon dioxide flux measurement systems. *Australian Journal of Botany* 56 (1):1.

Bastos, A., P. Friedlingstein, S. Sitch, C. Chen, A. Mialon, J.-P. Wigneron, V. K. Arora, P. R. Briggs, J. G. Canadell, P. Ciais, F. Chevallier, L. Cheng, C. Delire, V. Haverd, A. K. Jain, F. Joos, E. Kato, S. Lienert, D. Lombardozzi, J. R. Melton, R. Myneni, J. E. M. S. Nabel, J. Pongratz, B. Poulter, C. Rödenbeck, R. Séférian, H. Tian, C. van Eck, N. Viovy, N. Vuichard, A. P. Walker, A. Wiltshire, J. Yang, S. Zaehle, N. Zeng, and D. Zhu. 2018. Impact of the 2015/2016 El Niño on the terrestrial carbon cycle constrained by bottom-up and top-down approaches. *Philosophical Transactions of the Royal Society B: Biological Sciences* 373 (1760):20170304.

Beringer, J., L. B. Hutley, I. McHugh, S. K. Arndt, D. Campbell, H. A. Cleugh, J. Cleverly, V. Resco De Dios, D. Eamus, B. Evans, C. Ewenz, P. Grace, A. Griebel, V. Haverd, N. Hinko-Najera, A. Huete, P. Isaac, K. Kanniah, R. Leuning, M. J. Liddell, C. Macfarlane, W. Meyer, C. Moore, E. Pendall, A. Phillips, R. L. Phillips, S. M. Prober, N. Restrepo-Coupe, S. Rutledge, I. Schroder, R. Silberstein, P. Southall, M. S. Yee, N. J. Tapper, E. Van Gorsel, C. Vote, J. Walker, and T. Wardlaw. 2016. An introduction to the Australian and New Zealand flux tower network –OzFlux. *Biogeosciences* 13 (21):5895–5916.

Brodzik, M. J., B. Billingsley, T. Haran, B. Raup, and M. H. Savoie. 2012. EASE-Grid 2.0: Incremental but significant improvements for earth-gridded data sets. *ISPRS International Journal of Geo-Information* 1 (3):32–45.

Byrne, B., D. Wunch, D. B. Jones, K. Strong, F. Deng, I. Baker, P. Köhler, C. Frankenberg, J. Joiner, V. K. Arora, B. Badawy, A. B. Harper, T. Warneke, C. Petri, R. Kivi, and C. M. Roehl. 2018. Evaluating GPP and respiration estimates over northern midlatitude ecosystems using solar-induced fluorescence and atmospheric CO2 measurements. *Journal of Geophysical Research: Biogeosciences* 123 (9):2976–2997.

Cagnarini, C., E. Blyth, B. A. Emmett, C. D. Evans, R. I. Griffiths, A. Keith, L. Jones, I. Lebron, N. P. McNamara, J. Puissant, S. Reinsch, D. A. Robinson, E. C. Rowe, A. R. C. Thomas, S. M. Smart, J. Whitaker, and B. J. Cosby. 2019. Zones of influence for soil organic matter dynamics: A conceptual framework for data and models. *Global Change Biology* 25 (12):3996–4007.

Chiodi, A. M., and D. E. Harrison. 2013. El Niño impacts on seasonal U.S. Atmospheric circulation, temperature, and precipitation anomalies: The OLR-Event perspective. *Journal of Climate* 26 (3):822–837.

Collalti, A., and I. C. Prentice. 2019. Is NPP proportional to GPP? Waring's hypothesis 20 years on. *Tree Physiology* 39 (8):1473–1483.

Colliander, A., S. Chan, N. Das, S. Kim, S. Dunbar, T. Jackson, C. Derksen, J. McDonald, J. S. Kimball, E. Njoku, R. Reichle, and B. Weiss. 2014. *SMAP L2-L4 Data Products Calibration and Validation Plan*. Pasadena, CA: NASA Jet Propulsion Laboratory.

Cramer, W., D. W. Kicklighter, A. Bondeau, B. M. Iii, G. Churkina, B. Nemry, A. Ruimy, A. L. Schloss, and T. P. O. T. P. Intercomparison. 2001. Comparing global models of terrestrial net primary productivity (NPP): Overview and key results. *Global Change Biology* 5 (S1):1–15.

Endsley, K. A., M. Zhao, J. S. Kimball, and S. Devadiga. 2023a. Continuity of global MODIS terrestrial primary productivity estimates in the VIIRS era using model-data fusion. *Journal of Geophysical Research: Biogeosciences* 128 (9):e2023JG007457.

Endsley, K. A., J. S. Kimball, T. Kundig, R. H. Reichle, and J. V. Ardizzone. 2023b. *Validation Assessment for the Soil Moisture Active Passive (SMAP) Level 4 Carbon (L4_C) Data Product Version 7*. NASA.

Endsley, K. A., J. S. Kimball, and R. H. Reichle. 2022. Soil respiration phenology improves modeled phase of terrestrial net ecosystem exchange in northern hemisphere. *Journal of Advances in Modeling Earth Systems* 14 (2), 14, e2021MS002804, doi:10.1029/2021MS002804.

Endsley, K. A., J. S. Kimball, R. H. Reichle, and J. D. Watts. 2020. Satellite monitoring of global surface soil organic carbon dynamics using the SMAP Level 4 Carbon Product. *Journal of Geophysical Research: Biogeosciences* 125 (12), e2020JG006100, doi:10.1029/2020JG006100.

Euskirchen, E., G. Shaver, and S. Bret-Harte. 2016a. AmeriFlux AmeriFlux US-ICh Imnavait Creek Watershed Heath Tundra. https://www.osti.gov/servlets/purl/1246133/ (last accessed 28 July 2025).

———. 2016b. AmeriFlux AmeriFlux US-ICs Imnavait Creek Watershed Wet Sedge Tundra. https://www.osti.gov/servlets/purl/1246130/ (last accessed 28 July 2025).

———. 2016c. AmeriFlux AmeriFlux US-ICt Imnavait Creek Watershed Tussock Tundra. https://www.osti.gov/servlets/purl/1246131/ (last accessed 28 July 2025).

Fang, J., X. Lian, Y. Ryu, S. Jeong, C. Jiang, and P. Gentine. 2025. Long-term Continuous SIF-informed Photosynthesis Proxy reconstructed with MODIS surface reflectance (LCSPP-MODIS), 2001-2023. https://zenodo.org/doi/10.5281/zenodo.14614329 (last accessed 28 July 2025).

García-Herrera, R., J. M. Garrido-Perez, D. Barriopedro, C. Ordóñez, S. M. Vicente-Serrano, R. Nieto, L. Gimeno, R. Sorí, and P. Yiou. 2019. The European 2016/17 Drought. *Journal of Climate* 32 (11):3169–3187.

Hashimoto, H., R. R. Nemani, M. A. White, W. M. Jolly, S. C. Piper, C. D. Keeling, R. B. Myneni, and S. W. Running. 2004. El Niño-Southern Oscillation-induced variability in terrestrial carbon cycling. *Journal of Geophysical Research: Atmospheres* 109, D23110, doi:10.1029/2004JD004959.

Hengl, T., J. M. De Jesus, G. B. M. Heuvelink, M. R. Gonzalez, M. Kilibarda, A. Blagotić, W. Shangguan, M. N. Wright, X. Geng, B. Bauer-Marschallinger, M. A. Guevara, R. Vargas, R. A. MacMillan, N. H. Batjes, J. G. B. Leenaars, E. Ribeiro, I. Wheeler, S. Mantel, and B. Kempen. 2017. SoilGrids250m: Global gridded soil information based on machine learning. *PLoS ONE* 12 (2):1–40.

Hirata, R. 2021. Micrometeorological CO2 Flux Data at Tomakomai Flux Research Site (TMK). 16.1 MB. https://www.nies.go.jp/doi/10.17595/20210611.001-e.html (last accessed 28 July 2025).

Holmgren, M., M. Scheffer, E. Ezcurra, J. R. Gutiérrez, and G. M. J. Mohren. 2001. El Niño effects on the dynamics of terrestrial ecosystems. *Trends in Ecology & Evolution* 16 (2):89–94.

iSciences. 2016. Africa: Water Deficits across Northern Africa. iSciences. https://www.isciences.com/blog/2016/12/16/africa-water-deficits-across-northern-africa (last accessed 13 August 2025).

Jones, L. A., J. S. Kimball, R. H. Reichle, N. Madani, J. Glassy, J. V. Ardizzone, A. Colliander, J. Cleverly, A. R. Desai, D. Eamus, E. S. Euskirchen, L. Hutley, C. Macfarlane, and R. L. Scott. 2017. The SMAP Level 4 Carbon Product for Monitoring Ecosystem Land-Atmosphere CO2 Exchange. *IEEE Transactions on Geoscience and Remote Sensing* 55 (11):6517–6532.

Kimball, J. S., L. A. Jones, and J. P. Glassy. 2014. *Algorithm Theoretical Basis Document SMAP Level 4 Carbon Data Product (L4_C)*. NASA Jet Propulsion Laboratory (JPL).

Leuning, R., H. A. Cleugh, S. J. Zegelin, and D. Hughes. 2005. Carbon and water fluxes over a temperate Eucalyptus forest and a tropical wet/dry savanna in Australia: Measurements and comparison with MODIS remote sensing estimates. *Agricultural and Forest Meteorology* 129 (3-4):151–173.

Liu, Y., H. Xu, and Q. Sun. 2019. Learning rotation-invariant binary codes for efficient object detection from remote sensing images. *Journal of Applied Remote Sensing* 13 (03):1.

Nelson, J. A., S. Walther, F. Gans, B. Kraft, U. Weber, K. Novick, N. Buchmann, M. Migliavacca, G. Wohlfahrt, L. Šigut, A. Ibrom, D. Papale, M. Göckede, G. Duveiller, A. Knohl, L. Hörtnagl, R. L. Scott, J. Dušek, W. Zhang, Z. M. Hamdi, M. Reichstein, S. Aranda-Barranco, J. Ardö, M. Op De Beeck, D. Billesbach, D. Bowling, R. Bracho, C. Brümmer, G. Camps-Valls, S. Chen, J. R. Cleverly, A. Desai, G. Dong, T. S. El-Madany, E. S. Euskirchen, I. Feigenwinter, M. Galvagno, G. A. Gerosa, B. Gielen, I. Goded, S. Goslee, C. M. Gough, B. Heinesch, K. Ichii, M. A. Jackowicz-Korczynski, A. Klosterhalfen, S. Knox, H. Kobayashi, K.-M. Kohonen, M. Korkiakoski, I. Mammarella, M. Gharun, R. Marzuoli, R. Matamala, S. Metzger, L. Montagnani, G. Nicolini, T. O'Halloran, J.-M. Ourcival, M. Peichl, E. Pendall, B. Ruiz Reverter, M. Roland, S. Sabbatini, T. Sachs, M. Schmidt, C. R. Schwalm, A. Shekhar, R. Silberstein, M. L. Silveira, D. Spano, T. Tagesson, G. Tramontana, C. Trotta, F. Turco, T. Vesala, C. Vincke, D. Vitale, E. R. Vivoni, Y. Wang, W. Woodgate, E. A. Yepez, J. Zhang, D. Zona, and M. Jung. 2024. X-BASE: The first terrestrial carbon and water flux products from an extended data-driven scaling framework, FLUXCOM-X. *Biogeosciences* 21 (22):5079–5115.

Padarian, J., U. Stockmann, B. Minasny, and A. B. McBratney. 2022. Monitoring changes in global soil organic carbon stocks from space. *Remote Sensing of Environment* 281:113260.

Papale, D., M. Reichstein, M. Aubinet, E. Canfora, C. Bernhofer, W. Kutsch, B. Longdoz, S. Rambal, R. Valentini, T. Vesala, and D. Yakir. 2006. Towards a standardized processing of Net Ecosystem Exchange measured with eddy covariance technique: Algorithms and uncertainty estimation. *Biogeosciences* 3 (4):571–583.

Pastorello, G., C. Trotta, E. Canfora, H. Chu, D. Christianson, Y.-W. Cheah, C. Poindexter, J. Chen, A. Elbashandy, M. Humphrey, P. Isaac, D. Polidori, A. Ribeca, C. van Ingen, L. Zhang, B. Amiro, C. Ammann, M. A. Arain, J. Ardö, T. Arkebauer, S. K. Arndt, N. Arriga, M. Aubinet, M. Aurela, D. Baldocchi, A. Barr, E. Beamesderfer, L. B. Marchesini, O. Bergeron, J. Beringer,..., C. Bernhofer, D. Berveiller, D. Billesbach, T. A. Black, P. D. Blanken, G. Bohrer, J. Boike, P. V. Bolstad, D. Bonal, J.-M. Bonnefond, D. R. Bowling, R. Bracho, J. Brodeur, C. Brümmer, N. Buchmann, B. Burban, S. P. Burns, P. Buysse, P. Cale, M. Cavagna, P. Cellier, S. Chen, I. Chini, T. R. Christensen, J. Cleverly, A. Collalti, C. Consalvo, B. D. Cook, D. Cook, C. Coursolle, E. Cremonese, P. S. Curtis, E. D'Andrea, H. da Rocha, X. Dai, K. J. Davis, B. De Cinti, A. de Grandcourt, A. De Ligne, R. C. De Oliveira, N. Delpierre, A. R. Desai, C. M. Di Bella, P. di Tommasi, H. Dolman, F. Domingo, G. Dong, S. Dore, P. Duce, E. Dufrêne, A. Dunn, J. Dušek, D. Eamus, U. Eichelmann, H. A. M. ElKhidir, W. Eugster, C. M. Ewenz, B. Ewers, D. Famulari, S. Fares, I. Feigenwinter, A. Feitz, R. Fensholt, G. Filippa, M. Fischer, J. Frank, M. Galvagno, et al. 2020. The FLUXNET2015 dataset and the ONEFlux processing pipeline for eddy covariance data. *Scientific Data* 7 (1):225.

Restrepo-Coupe, N., H. R. da Rocha, L. R. Hutyra, A. C. de Araujo, L. S. Borma, B. Christoffersen, O. Cabral, P. B. de Camargo, F. L. Cardoso, A. C. L. Costa, D. R. Fitzjarrald, M. L. Goulden, B. Kruijt, J. M. F. Maia, Y. S. Malhi, A. O. Manzi, S. D. Miller, A. D. Nobre, C. von Randow, L. D. Abreu Safaj, R. K. Sakai, J. Tota, S. C. Wofsy, F. B. Zanchi, and S. R. Saleska. 2021. Large Scale Biosphere-Atmosphere Experiment (LBA-ECO) CD-32 Flux Tower Network Data Compilation, Brazilian Amazon: 1999-2006, V2.

Sitch, S., M. O'Sullivan, E. Robertson, P. Friedlingstein, C. Albergel, P. Anthoni, A. Arneth, V. K. Arora, A. Bastos, V. Bastrikov, N. Bellouin, J. G. Canadell, L. Chini, P. Ciais, S. Falk, I. Harris, G. Hurtt, A. Ito, A. K. Jain, M. W. Jones, F. Joos, E. Kato, D. Kennedy, K. Klein Goldewijk, E. Kluzek, J. Knauer, P. J. Lawrence, D. Lombardozzi, J. R. Melton, J. E. M. S. Nabel, N. Pan, P. Peylin, J. Pongratz, B. Poulter, T. M. Rosan, Q. Sun, H. Tian, A. P. Walker, U. Weber, W. Yuan, X. Yue, and S. Zaehle. 2024.

Trends and drivers of terrestrial sources and sinks of carbon dioxide: An overview of the TRENDY project. *Global Biogeochemical Cycles* 38 (7):e2024GB008102.

Takagi, K. 2014. Micrometeorological CO2 Flux Data at Teshio CC-LaG Experiment site (TSE). 77.7 MB. https://www.nies.go.jp/doi/10.17595/20221006.001-e.html (last accessed 28 July 2025).

Takahashi, Y. 2021. Micrometeorological CO2 Flux Data at Fuji Hokuroku Flux Observation Site (FHK). 60 MB. https://www.nies.go.jp/doi/10.17595/20210730.001-e.html (last accessed 28 July 2025).

Ukkola, A., G. Abramowitz, and M. De Kauwe. 2021. A flux tower dataset tailored for land model evaluation. *Earth System Science Data Discussions*:1–20.

Wardlaw, T., and A. Phillips. 2021. Warra Flux Data Collection. Version 1.0. https://portal.tern.org.au/metadata/TERN/227eb5a0-ad1e-451d-b41f-ebab73411bd6.

Woodgate, W. 2013. Tumbarumba OzFlux tower site. http://hdl.handle.net/102.100.100/14241.

Wurster, P., M. P. Maneta, J. S. Kimball, K. A. Endsley, and S. Beguería. 2021. Monitoring crop status in the United States using the SMAP Level 4 Carbon product. *Frontiers in Big Data* 3, doi:10.3389/fdata.2020.597720.

Xia, Y., J. Sanderman, J. D. Watts, M. B. Machmuller, A. L. Mullen, C. Rivard, A. Endsley, H. Hernandez, J. Kimball, S. A. Ewing, M. Litvak, T. Duman, P. Krishnan, T. Meyers, N. A. Brunsell, B. Mohanty, H. Liu, Z. Gao, J. Chen, M. Abraha, R. L. Scott, G. N. Flerchinger, P. E. Clark, P. C. Stoy, A. M. Khan, E. N. J. Brookshire, Q. Zhang, D. R. Cook, T. Thienelt, B. Mitra, M. Mauritz-Tozer, C. E. Tweedie, M. S. Torn, and D. Billesbach. 2025. Coupling remote sensing with a process model for the simulation of rangeland carbon dynamics. *Journal of Advances in Modeling Earth Systems* 17 (3), e2024MS004342.

Zhang, Y., M. P. Dannenberg, T. Hwang, and C. Song. 2019. El Niño-Southern Oscillation-Induced Variability of Terrestrial Gross Primary Production During the Satellite Era. *Journal of Geophysical Research: Biogeosciences* 124 (8):2419–2431.

Zhang, Y., J. Joiner, S. Hamed Alemohammad, S. Zhou, and P. Gentine. 2018. A global spatially contiguous solar-induced fluorescence (CSIF) dataset using neural networks. *Biogeosciences* 15 (19):5779–5800.

Zhu, Z., S. Piao, Y. Xu, A. Bastos, P. Ciais, and S. Peng. 2017. The effects of teleconnections on carbon fluxes of global terrestrial ecosystems: Effects of Teleconnections on C Fluxes. *Geophysical Research Letters* 44 (7):3209–3218.

Previous Volumes in This Series

Volume 1 September 1994	*Documentation of the Goddard Earth Observing System (GEOS) general circulation model - Version 1* L.L. Takacs, A. Molod, and T. Wang
Volume 2 October 1994	*Direct solution of the implicit formulation of fourth order horizontal diffusion for gridpoint models on the sphere* Y. Li, S. Moorthi, and J.R. Bates
Volume 3 December 1994	*An efficient thermal infrared radiation parameterization for use in general circulation models* M.-D. Chou and M.J. Suarez
Volume 4 January 1995	*Documentation of the Goddard Earth Observing System (GEOS) Data Assimilation System - Version 1* James Pfaendtner, Stephen Bloom, David Lamich, Michael Seablom, Meta Sienkiewicz, James Stobie, and Arlindo da Silva
Volume 5 April 1995	*Documentation of the Aries-GEOS dynamical core: Version 2* Max J. Suarez and Lawrence L. Takacs
Volume 6 April 1995	*A Multiyear Assimilation with the GEOS-1 System: Overview and Results* Siegfried Schubert, Chung-Kyu Park, Chung-Yu Wu, Wayne Higgins, Yelena Kondratyeva, Andrea Molod, Lawrence Takacs, Michael Seablom, and Richard Rood
Volume 7 September 1995	*Proceedings of the Workshop on the GEOS-1 Five-Year Assimilation* Siegfried D. Schubert and Richard B. Rood
Volume 8 March 1996	*Documentation of the Tangent Linear Model and Its Adjoint of the Adiabatic Version of the NASA GEOS-1 C-Grid GCM: Version 5.2* Weiyu Yang and I. Michael Navon

Volume 9 March 1996	*Energy and Water Balance Calculations in the Mosaic LSM* Randal D. Koster and Max J. Suarez
Volume 10 April 1996	*Dynamical Aspects of Climate Simulations Using the GEOS General Circulation Model* Lawrence L. Takacs and Max J. Suarez
Volume 11 May 1997	*Documentation of the Tangent Linear and Adjoint Models of the Relaxed Arakawa-Schubert Moisture Parameterization Package of the NASA GEOS-1 GCM (Version 5.2)* Weiyu Yang, I. Michael Navon, and Ricardo Todling
Volume 12 August 1997	*Comparison of Satellite Global Rainfall Algorithms* Alfred T.C. Chang and Long S. Chiu
Volume 13 December 1997	*Interannual Variability and Potential Predictability in Reanalysis Products* Wie Ming and Siegfried D. Schubert
Volume 14 August 1998	*A Comparison of GEOS Assimilated Data with FIFE Observations* Michael G. Bosilovich and Siegfried D. Schubert
Volume 15 June 1999	*A Solar Radiation Parameterization for Atmospheric Studies* Ming-Dah Chou and Max J. Suarez
Volume 16 November 1999	*Filtering Techniques on a Stretched Grid General Circulation Model* Lawrence Takacs, William Sawyer, Max J. Suarez, and Michael S. Fox-Rabinowitz
Volume 17 July 2000	*Atlas of Seasonal Means Simulated by the NSIPP-1 Atmospheric GCM* Julio T. Bacmeister, Philip J. Pegion, Siegfried D. Schubert, and Max J. Suarez

Volume 18
December 2000

An Assessment of the Predictability of Northern Winter Seasonal Means with the NSIPP1 AGCM

Philip J. Pegion, Siegfried D. Schubert, and Max J. Suarez

Volume 19
July 2001

A Thermal Infrared Radiation Parameterization for Atmospheric Studies

Ming-Dah Chou, Max J. Suarez, Xin-Zhong Liang, and Michael M.-H. Yan

Volume 20
August 2001

The Climate of the FVCCM-3 Model

Yehui Chang, Siegfried D. Schubert, Shian-Jiann Lin, Sharon Nebuda, and Bo-Wen Shen

Volume 21
September 2001

Design and Implementation of a Parallel Multivariate Ensemble Kalman Filter for the Poseidon Ocean General Circulation Model

Christian L. Keppenne and Michele M. Rienecker

Volume 22
August 2002

A Coupled Ocean-Atmosphere Radiative Model for Global Ocean Biogeochemical Models

Watson W. Gregg

Volume 23
November 2002

Prospects for Improved Forecasts of Weather and Short-term Climate Variability on Subseasonal (2-Week to 2-Month) Time Scales

Siegfried D. Schubert, Randall Dole, Huang van den Dool, Max J. Suarez, and Duane Waliser

Volume 24
July 2003

Temperature Data Assimilation with Salinity Corrections: Validation for the NSIPP Ocean Data Assimilation System in the Tropical Pacific Ocean, 1993–1998

Alberto Troccoli, Michele M. Rienecker, Christian L. Keppenne, and Gregory C. Johnson

Volume 25
December 2003

Modeling, Simulation, and Forecasting of Subseasonal Variability

Duane Waliser, Siegfried D. Schubert, Arun Kumar, Klaus Weickmann, and Randall Dole

Volume 26
April 2005

Documentation and Validation of the Goddard Earth Observing System (GEOS) Data Assimilation System – Version 4

Senior Authors: S. Bloom, A. da Silva and D. Dee

Contributing Authors: M. Bosilovich, J-D. Chern, S. Pawson, S. Schubert, M. Sienkiewicz, I. Stajner, W-W. Tan, and M-L. Wu

Volume 27
December 2008

The GEOS-5 Data Assimilation System - Documentation of Versions 5.0.1, 5.1.0, and 5.2.0.

M.M. Rienecker, M.J. Suarez, R. Todling, J. Bacmeister, L. Takacs, H.-C. Liu, W. Gu, M. Sienkiewicz, R.D. Koster, R. Gelaro, I. Stajner, and J.E. Nielsen

Volume 28
April 2012

The GEOS-5 Atmospheric General Circulation Model: Mean Climate and Development from MERRA to Fortuna

Andrea Molod, Lawrence Takacs, Max Suarez, Julio Bacmeister, In-Sun Song, and Andrew Eichmann

Volume 29
June 2012

Atmospheric Reanalyses – Recent Progress and Prospects for the Future.

A Report from a Technical Workshop, April 2010

Michele M. Rienecker, Dick Dee, Jack Woollen, Gilbert P. Compo, Kazutoshi Onogi, Ron Gelaro, Michael G. Bosilovich, Arlindo da Silva, Steven Pawson, Siegfried Schubert, Max Suarez, Dale Barker, Hirotaka Kamahori, Robert Kistler, and Suranjana Saha

Volume 30
December 2012

The GEOS-iODAS: Description and Evaluation

Guillaume Vernieres, Michele M. Rienecker, Robin Kovach and Christian L. Keppenne

Volume 31
March 2013

Global Surface Ocean Carbon Estimates in a Model Forced by MERRA

Watson W. Gregg, Nancy W. Casey and Cécile S. Rousseaux

Volume 32
March 2014

Estimates of AOD Trends (2002-2012) over the World's Major Cities based on the MERRA Aerosol Reanalysis

Simon Provencal, Pavel Kishcha, Emily Elhacham, Arlindo M. da Silva, and Pinhas Alpert

Volume 33
August 2014

The Effects of Chlorophyll Assimilation on Carbon Fluxes in a Global Biogeochemical Model

Cécile S. Rousseaux and Watson W. Gregg

Volume 34
September 2014

Background Error Covariance Estimation using Information from a Single Model Trajectory with Application to Ocean Data Assimilation into the GEOS-5 Coupled Model

Christian L. Keppenne, Michele M. Rienecker, Robin M. Kovach, and Guillaume Vernieres

Volume 35
December 2014

Observation-Corrected Precipitation Estimates in GEOS-5

Rolf H. Reichle and Qing Liu

Volume 36
March 2015

Evaluation of the 7-km GEOS-5 Nature Run

Ronald Gelaro, William M. Putman, Steven Pawson, Clara Draper, Andrea Molod, Peter M. Norris, Lesley Ott, Nikki Prive, Oreste Reale, Deepthi Achuthavarier, Michael Bosilovich, Virginie Buchard, Winston Chao, Lawrence Coy, Richard Cullather, Arlindo da Silva, Anton Darmenov, Ronald M. Errico, Marangelly Fuentes, Min-Jeong Kim, Randal Koster, Will McCarty, Jyothi Nattala, Gary Partyka, Siegfried Schubert, Guillaume Vernieres, Yuri Vikhliaev, and Krzysztof Wargan

Volume 37
March 2015

Maintaining Atmospheric Mass and Water Balance within Reanalysis

Lawrence L. Takacs, Max Suarez, and Ricardo Todling

Volume 38
September 2015

The Quick Fire Emissions Dataset (QFED) – Documentation of versions 2.1, 2.2 and 2.4

Anton S. Darmenov and Arlindo da Silva

Volume 39
September 2015

Land Boundary Conditions for the Goddard Earth Observing System Model Version 5 (GEOS-5) Climate Modeling System - Recent Updates and Data File Descriptions

Sarith Mahanama, Randal Koster, Gregory Walker, Lawrence Takacs, Rolf Reichle, Gabrielle De Lannoy, Qing Liu, Bin Zhao, and Max Suarez

Volume 40	*Soil Moisture Active Passive (SMAP) Project Assessment Report for the Beta-Release L4_SM Data Product*
October 2015	Rolf H. Reichle, Gabrielle J. M. De Lannoy, Qing Liu, Andreas Colliander, Austin Conaty, Thomas Jackson, John Kimball, and Randal D. Koster
Volume 41	*GDIS Workshop Report*
October 2015	Siegfried Schubert, Will Pozzi, Kingtse Mo, Eric Wood, Kerstin Stahl, Mike Hayes, Juergen Vogt, Sonia Seneviratne, Ron Stewart, Roger Pulwarty, and Robert Stefanski
Volume 42	*Soil Moisture Active Passive (SMAP) Project Calibration and Validation for the L4_C Beta-Release Data Product*
November 2015	John Kimball, Lucas Jones, Joseph Glassy, E. Natasha Stavros, Nima Madani, Rolf Reichle, Thomas Jackson, and Andreas Colliander
Volume 43	*MERRA-2: Initial Evaluation of the Climate*
September 2015	Michael G. Bosilovich, Santha Akella, Lawrence Coy, Richard Cullather, Clara Draper, Ronald Gelaro, Robin Kovach, Qing Liu, Andrea Molod, Peter Norris, Krzysztof Wargan, Winston Chao, Rolf Reichle, Lawrence Takacs, Yury Vikhliaev, Steve Bloom, Allison Collow, Stacey Firth, Gordon Labow, Gary Partyka, Steven Pawson, Oreste Reale, Siegfried Schubert, and Max Suarez
Volume 44	*Estimation of the Ocean Skin Temperature using the NASA GEOS Atmospheric Data Assimilation System*
February 2016	Santha Akella, Ricardo Todling, Max Suarez
Volume 45	*The MERRA-2 Aerosol Assimilation*
October 2016	C. A. Randles, A. M. da Silva, V. Buchard, A. Darmenov, P. R. Colarco, V. Aquila, H. Bian, E. P. Nowottnick, X. Pan, A. Smirnov, H. Yu, and R. Govindaraju
Volume 46	*The MERRA-2 Input Observations: Summary and Assessment*
October 2016	Will McCarty, Lawrence Coy, Ronald Gelaro, Albert Huang, Dagmar Merkova, Edmond B. Smith, Meta Sienkiewicz, and Krzysztof Wargan

Volume 47
May 2017

An Evaluation of Teleconnections Over the United States in an Ensemble of AMIP Simulations with the MERRA-2 Configuration of the GEOS Atmospheric Model.

Allison B. Marquardt Collow, Sarith P. Mahanama, Michael G. Bosilovich, Randal D. Koster, and Siegfried D. Schubert

Volume 48
July 2017

Description of the GMAO OSSE for Weather Analysis Software Package: Version 3

Ronald M. Errico, Nikki C. Prive, David Carvalho, Meta Sienkiewicz, Amal El Akkraoui, Jing Guo, Ricardo Todling, Will McCarty, William M. Putman, Arlindo da Silva, Ronald Gelaro, and Isaac Moradi

Volume 49
March 2018

Preliminary Evaluation of Influence of Aerosols on the Simulation of Brightness Temperature in the NASA Goddard Earth Observing System Atmospheric Data Assimilation System

Jong Kim, Santha Akella, Will McCarty, Ricardo Todling, and Arlindo M. da Silva

Volume 50
March 2018

The GMAO Hybrid Ensemble-Variational Atmospheric Data Assimilation System: Version 2.0

Ricardo Todling and Amal El Akkraoui

Volume 51
July 2018

The Atmosphere-Ocean Interface Layer of the NASA Goddard Earth Observing System Model and Data Assimilation System

Santha Akella and Max Suarez

Volume 52
July 2018

Soil Moisture Active Passive (SMAP) Project Assessment Report for Version 4 of the L4_SM Data Product

Rolf H. Reichle, Qing Liu, Randal D. Koster, Joe Ardizzone, Andreas Colliander, Wade Crow, Gabrielle J. M. De Lannoy, and John Kimball

Volume 53
October 2019

Ensemble Generation Strategies Employed in the GMAO GEOS-S2S Forecast System

Siegfried Schubert, Anna Borovikov, Young-Kwon Lim, and Andrea Molod

Volume 54
August 2020

Position Estimation of Atmospheric Motion Vectors for Observation System Simulation Experiments

David Carvalho and Will McCarty

Volume 55
February 2021

A Phenomenon-Based Decomposition of Model-Based Estimates of Boreal Winter ENSO Variability

Schubert, Siegfried, Young-Kwon Lim, Andrea Molod, and Allison Collow

Volume 56
June 2021

Validation Assessment for the Soil Moisture Active Passive (SMAP) Level 4 Carbon (L4_C) Data Product Version 5

John S. Kimball, K. Arthur Endsley, Tobias Kundig, Joseph Glassy, Rolf H. Reichle, and Joseph V. Ardizzone

Volume 57
July 2021

Tendency Bias Correction in the GEOS AGCM

Yehui Chang, Siegfried Schubert, Randal Koster, and Andrea Molod

Volume 58
August 2021

Soil Moisture Active Passive (SMAP) Project Assessment Report for Version 5 of the L4_SM Data Product

Rolf H. Reichle, Qing Liu, Randal D. Koster, Joseph V. Ardizzone, Andreas Colliander, Wade Crow, Gabrielle J. M. De Lannoy, and John S. Kimball

Volume 59
November 2021

Observation-Corrected Land Surface Precipitation for the SMAP Level 4 Soil Moisture (Version 6) Product and the GEOS R21C Reanalysis

Rolf H. Reichle and Qing Liu

Volume 60
January 2022

Soil Moisture Active Passive (SMAP) Project Assessment Report for Version 6 of the L4_SM Data Product

Rolf H. Reichle, Qing Liu, Randal D. Koster, Joseph V. Ardizzone, Andreas Colliander, Wade Crow, Gabrielle J. M. De Lannoy, and John S. Kimball

Volume 61
April 2022

Validation Assessment for the Soil Moisture Active Passive (SMAP) Level 4 Carbon (L4_C) Data Product Version 6

John S. Kimball, K. Arthur Endsley, Tobias Kundig, Joseph Glassy, Rolf H. Reichle, Joseph V. Ardizzone

Volume 62
September 2022

Climate Characteristics of the Atmospheric Analysis Increments from the GEOS S2S V3 AOGCM Replayed to MERRA-2

Yehui Chang, Siegfried Schubert, Randal Koster, Andrea Molod, Young-Kwon Lim

Volume 63
October 2022

GEOS aerosol optical table calculation package GEOSmie

Osku Kemppinen, Peter Colarco, Patricia Castellanos

Volume 64
March 2023

Soil Moisture Active Passive (SMAP) Project Assessment Report for Version 7 of the L4_SM Data Product

Rolf Reichle, Qing Liu, Joseph Ardizzone, Michel Bechtold, Wade Crow, Gabrielle De Lannoy, John Kimball, Randal Koster

Volume 65
June 2023

Validation Assessment for the Soil Moisture Active Passive (SMAP) Level 4 Carbon (L4_C) Data Product Version 7

John S. Kimball, K. Arthur Endsley, Tobias Kundig, Rolf H. Reichle, Joseph V. Ardizzone